HHS Public Access

Author manuscript

Neurobiol Dis. Author manuscript; available in PMC 2017 January 01.

Published in final edited form as:

Neurobiol Dis. 2016 January ; 85: 81–92. doi:10.1016/j.nbd.2015.10.005.

Reduction of thalamic and cortical I_h by deletion of TRIP8b produces a mouse model of human absence epilepsy

Robert J. Heuermann[a,*], **Thomas C. Jaramillo, PhD**[a,e,*], **Shui-Wang Ying, PhD**[c], **Benjamin A. Suter**[b], **Kyle A. Lyman**[a], **Ye Han, PhD**[a], **Alan S. Lewis, MD, PhD**[a,f], **Thomas G. Hampton, PhD**[d], **Gordon M. G. Shepherd, MD, PhD**[b], **Peter A. Goldstein, MD**[c], and **Dane M. Chetkovich**[a,b]

Robert J. Heuermann: r-heuermann@northwestern.edu; Thomas C. Jaramillo: tom.jaramillo@utsouthwestern.edu; Shui-Wang Ying: yingsw200@gmail.com; Benjamin A. Suter: ben.suter@gmail.com; Kyle A. Lyman: kyle-lyman@northwestern.edu; Ye Han: ye-han@northwestern.edu; Alan S. Lewis: alan.lewis@yale.edu; Thomas G. Hampton: hampton@mousespecifics.com; Gordon M. G. Shepherd: g-shepherd@northwestern.edu; Peter A. Goldstein: pag2014@med.cornell.edu

[a]Davee Department of Neurology and Clinical Neurosciences, Feinberg School of Medicine, Northwestern University, 303 E. Chicago Ave., Ward Building, Room 10-201, Chicago, IL 60611

[b]Department of Physiology, Feinberg School of Medicine, Northwestern University, 303 E. Chicago Ave., Ward Building, Room 10-201, Chicago, IL 60611

[c]C.V. Starr Laboratory for Molecular Neuropharmacology, Department of Anesthesiology, Weill Medical College of Cornell University, 1300 York Ave., Room A-1050, New York, New York 10021

[d]Mouse Specifics, Inc., 2 Central Street, Level 1 Suite 1, Framingham MA 01701 USA

Abstract

Absence seizures occur in several types of human epilepsy and result from widespread, synchronous feedback between the cortex and thalamus that produces brief episodes of loss of consciousness. Genetic rodent models have been invaluable for investigating the pathophysiological basis of these seizures. Here, we identify tetratricopeptide-containing Rab8b-interacting protein (TRIP8b) knockout mice as a new model of absence epilepsy, featuring spontaneous spike-wave discharges on electroencephalography (EEG) that are the electrographic hallmark of absence seizures. TRIP8b is an auxiliary subunit of the hyperpolarization-activated

Corresponding author and address: Dane M. Chetkovich, MD, PhD, Davee Department of Neurology and Clinical Neuroscience, Feinberg School of Medicine, Northwestern University, 303 East Chicago Avenue, Ward 10-201, Chicago, IL 60611-3008, 312-503-4362 Office, 312-503-0872 Fax, d-chetkovich@northwestern.edu.

[*]These authors contributed equally to this work

[e]Present address: Department of Neurology, University of Texas Southwestern Medical Center, 5323 Harry Hines Blvd. ND4.504, Dallas, TX 75390-8813, USA

[f]Present address: Department of Psychiatry, Yale University School of Medicine, 34 Park Street, 3rd Floor Research, New Haven, CT 06508, USA

Financial Interests:

TGH holds an equity stake in the company Mouse Specifics, Inc., a provider of the gait analysis and ECG monitoring equipment described in the Methods.

cyclic-nucleotide-gated (HCN) channels, which have previously been implicated in the pathogenesis of absence seizures. In contrast to mice lacking the pore-forming HCN channel subunit HCN2, TRIP8b knockout mice exhibited normal cardiac and motor function and a less severe seizure phenotype. Evaluating the circuit that underlies absence seizures, we found that TRIP8b knockout mice had significantly reduced HCN channel expression and function in thalamic-projecting cortical layer 5b neurons and thalamic relay neurons, but preserved function in inhibitory neurons of the reticular thalamic nucleus. Our results expand the known roles of TRIP8b and provide new insight into the region-specific functions of TRIP8b and HCN channels in constraining cortico-thalamo-cortical excitability.

Keywords

TRIP8b; HCN channels; I_h; absence epilepsy; neocortex; thalamus

Introduction

Absence seizures are characterized by brief episodes of loss of consciousness without prominent motor involvement that are accompanied by characteristic 2–4 Hz spike-wave discharges (SWDs) seen across all cortical leads on EEG. These seizures occur in several human epilepsy syndromes, including the most common pediatric epilepsy, childhood absence epilepsy (Jallon et al., 2001). Although often misconstrued as a benign condition that spontaneously remits in adolescence, many children with childhood absence epilepsy suffer long-term cognitive and psychosocial deficits (Pavone et al., 2001). Existing pharmacological therapies fail to adequately control seizures in many patients, and even when successful these drugs themselves often induce adverse cognitive and behavioral side-effects (Glauser et al., 2010). Thus, there is need for more targeted therapeutic options for absence seizures, which will in turn require improved understanding of the underlying pathophysiology.

Absence seizures have long been known to arise from aberrant activity in the thalamocortical network (reviewed in Avoli, 2012). Existing evidence suggests SWDs initiate focally in the cortex (Meeren et al., 2002; Polack et al., 2007), followed by reverberant feedback between thalamocortical (TC) neurons in various thalamic nuclei and GABAergic cells of the reticular thalamic nucleus (RTN) that rapidly generalizes across broad areas of the thalamus and cortex (Huguenard and McCormick, 2007). A growing number of genetic rodent models of absence epilepsy have greatly enhanced our understanding of the finer-scale cellular and molecular abnormalities that lead to cortico-thalamo-cortical hyperexcitability (reviewed in Deng et al., 2014). Two of these models resulted from the targeted (Ludwig et al., 2003) and spontaneous (Chung et al., 2009) disruption of the *Hcn2* gene in mice, which encodes a pore-forming subunit of the hyperpolarization-activated cyclic-nucleotide-gated (HCN) ion channel family. HCN channels pass a non-selective Na^+/K^+ current (I_h) that activates near or below typical neuronal resting potentials and does not inactivate (Biel et al., 2009). Intracellular binding of cAMP shifts activation to more positive potentials, making HCN channels important effectors of neuromodulatory signaling. In TC neurons, the depolarizing influence of I_h

inactivates T-type Ca^{2+} channels and promotes the transition from oscillatory bursts of action potentials to a tonic firing mode, which is associated with wakefulness. Conversely, TC neuron burst firing is increased during unconscious states, including slow-wave sleep (Llinás and Steriade, 2006) and absence seizures (Staak and Pape, 2001; Budde et al., 2005; Beenhakker and Huguenard, 2009).

Our group previously reported that mice lacking tetratricopeptide-repeat-containing Rab8b-interacting protein (TRIP8b), an auxiliary subunit of HCN channels, demonstrate substantial downregulation of I_h in CA1 pyramidal neurons, but exhibit only subtle behavioral changes (Lewis et al., 2011). However, we suspected that loss of TRIP8b might induce occult epileptiform activity similar to loss of HCN2. Here, we report spontaneous SWDs associated with behavioral arrest in TRIP8b knockout mice, reminiscent of human absence epilepsy. These mice do not have additional neurological or cardiac impairments as seen in mice lacking HCN2. Using biochemical, immunohistochemical, and electrophysiological techniques, we demonstrate markedly reduced HCN channel function in neocortical pyramidal neurons and TC neurons, but preserved I_h in the RTN. Our findings establish the TRIP8b knockout mouse as a novel model of absence epilepsy that provides new insights into the importance of I_h in thalamocortical networks.

Materials and Methods

Mice

All animal experiments were performed according to protocols approved by the Institutional Animal Care and Use Committees of Northwestern University and Cornell University. Generation of total body TRIP8b knockout mice used in this study has been previously described (Lewis et al., 2011).

Animal surgery, EEG recording

A more detailed procedure of animal surgery for long-term recording in freely moving mice has been previously described (Shin et al., 2008). Briefly, mice were anesthetized with a mixture of ketamine (80 mg/kg) and xylazine (9 mg/kg). A prefabricated mouse headmount (Pinnacle Technologies) was fastened onto the skull with 4 electrodes contacting the dura, two placed 1 mm anterior to bregma and two placed 7 mm anterior to bregma, each being 1.5 mm lateral to the central sulcus. Mice were allowed 7 days to recover then placed in recording chambers for continuous 24-hr simultaneous video and EEG recordings. EEG/video analysis was performed offline by manually scrolling through 60 s epochs of EEG data to detect seizure activity. SWDs were scored for each animal only if the EEG demonstrated a distinct 3–8 Hz spike-wave morphology, with amplitudes at least 2 times higher than baseline.

Animal pharmacology

After 1 hr of habituation to the recording chamber, a 2 hr period of baseline recording was carried out before injections. Injections and dosages used were as follows: ethosuximide (200 mg/kg), carbamazepine (20 mg/kg), or γ-butyrolactone (100 mg/kg). All were dissolved in normal saline and injected intraperitoneally. Following injections, a video-EEG

recording period (≥ 80 min) was conducted. EEGs were analyzed thereafter for the presence of SWDs as described above. EEG analysis was conducted by an investigator blinded to mouse genotype.

Rotarod

Motor coordination in a group of 21 mice (7 wild-type (WT), 7 TRIP8b KO, and 7 *apathetic* (HCN2 null mice)) between 6–11 weeks of age was assessed by placing the mice on a rotating-rod apparatus (Ugo Basile) that was set to either maintain a fixed speed (24 or 40 rpm) or to accelerate speed (from 4 to 40 rpm). In both the fixed and accelerating rotarod experiments, mice were tested in a single trial, and the amount of time before a mouse fell off the rotarod was recorded. The maximum time recorded was 10 min per mouse. If a mouse held onto the rotating rod for one complete revolution it was scored as a fall.

DigiGait

Gait dynamics were assessed on a group of 17 male mice (4 WT, 9 TRIP8b KO, 4 *apathetic*) between the ages of 6–8 weeks and described in detail previously (Hampton et al., 2004). Briefly, mice were place onto a transparent treadmill with a high-speed digital camera mounted underneath. Mice walked on the treadmill belt at a set speed of 17 cm/s. Images were collected at 150 frames per second and were converted to gray-scale to measure the area of pixels of the moving paws relative to the belt and the camera. Stride length and stance width were determine based on the sequential placement of the paws on the treadmill belt, and the distances between the fore paws and hind paws at peak stance, as previously described (Hampton et al., 2004).

ECG recordings

ECGs were recorded non-invasively on a group of 10 male mice (4 WT, 3 TRIP8b KO, 3 *apathetic*) between the ages of 6–8 weeks as described in detail previously (Chu et al., 2001). Briefly, mice were removed from their cages and placed on the ECGenie recording platform (Mouse Specifics, Inc., Boston, MA, USA). Each mouse was allowed to acclimate to the ECG platform for 10 minutes. ECG signals were then recorded and digitized at a sampling rate of 2000 samples/sec. Only data from continuous recordings were analyzed. Each signal was analyzed using e-MOUSE software (Mouse Specifics, Inc., Boston, MA, USA) (Chu et al., 2001; Hampton et al., 2012). E-MOUSE incorporates Fourier analysis and linear time-invariant digital filtering of frequencies below 2 Hz and above 100 Hz to minimize environmental signal disturbances. The software uses a peak detection algorithm to find the peak of the R-waves and to calculate heart rate. Heart rate variability was calculated as the mean of the differences between sequential heart rates for the complete set of ECG signals for each genotype.

Western blotting

Primary antibodies and concentrations used for western blotting: rabbit α-HCN1 (1:1,000) and rabbit α-TRIP8b (1:10,000) (Lewis et al., 2011); guinea pig α-HCN2 (1:1,000) (Shin et al., 2006); mouse α-HCN3 (1:1,000, NeuroMab); guinea pig α-HCN4 (1:1,000) (Shin et al., 2008); rabbit α-GluR1 (1:1,000, Millipore); and mouse α-βIII-tubulin (1:3,000, Sigma).

Primary antibodies were diluted in blocking solution containing 5% milk and 0.1% Tween-20 in TBS. Western blotting was performed as previously described (Lewis et al., 2009). Band intensities were quantified using NIH ImageJ software and normalized to the βIII-tubulin signal for each sample.

Surface biotinylation

Male mice ages 10–16 weeks were deeply anesthetized with isoflurane and rapidly decapitated. Brains were removed and placed in a vibratome chamber with ice-cold artificial cerebrospinal fluid (ACSF) containing (in mM) 124 NaCl, 3 KCl, 2 $CaCl_2$, 25 $NaHCO_3$, 1.1 NaH_2PO_4, 2 $MgSO_4$, and 10 D-glucose, and equilibrated with 95% O_2 and 5% CO_2 to yield a pH 7.4. Brains were sectioned at 350 μm and thalamic tissue corresponding to regions below the hippocampus, adjacent to the lateral ventricles and above the apex of the third ventricle was dissected and placed in a 6-well culture tray adapted to operate as a continuously gasified chamber (95% O_2 and 5% CO_2). Sections were washed twice for 5 min with ice-cold ACSF and then incubated in ACSF containing 2mg/mL sulfo-NHS-LC-biotin (Sigma). After 45 min of incubation, slices were washed twice with PBS containing 20 mM NH_4Cl (Sigma) to quench excess reactive biotin. Slices were then transferred to a microcentrifuge tube and immediately sonicated in 500 μL of lysis buffer (1% Triton X-100, 0.1% SDS, 1mM EDTA, 50mM NaCl, 20mM Tris, pH 7.5, and protease inhibitor cocktail (Roche)). Biotinylated samples were precipitated with ultra-link immobilized streptavidin beads (Pierce) and eluted with sample buffer for subsequent western blotting. The percentage of surface expression for each sample was obtained by normalizing the biotinylated fraction to the input.

Thalamocortical electrophysiology

Brain slice preparations have previously been described (Ying and Goldstein, 2005). Briefly, mice (P60–95) were anesthetized with isoflurane (or by pentobarbital in about 50% of mice used), and horizontal brain slices (300 μm) prepared. Whole-cell voltage-clamp recordings of neurons in the ventrobasal complex were obtained (Ying et al., 2006). All recordings were carried out at 32°C, except for the experiments on current density, which were made at 24°C to improve membrane stability during 10 s steps to −130 mV. Slices were perfused with ACSF containing (in mM): NaCl 124, $NaHCO_3$ 26, KCl 5, NaH_2PO_4 1.25, $MgCl_2$ 2; $CaCl_2$ 2, D-glucose 18, and tetrodotoxin 0.001. For analyses of I_h current density, an "I_h-isolation solution" was used (ACSF to which the following were added, in mM: 4-aminopyridine (4-AP) 0.1, $BaCl_2$ 1, $NiCl_2$ 0.1, D-2-amino-5-phosphonovaleric acid (AP5) 0.04, and 6-cyano-7-nitroquinoxaline-2,3-dione (CNQX) 0.02). The intracellular solution contained (in mM): K^+-gluconate 135, NaCl 5, HEPES 10, EGTA 0.5, ATP-Mg^{2+} 2, GTP-Na^+ 0.3, Na^+-phosphocreatine 5; the pH was adjusted to 7.3 with KOH. Data were obtained with a Multiclamp 700B amplifier (Molecular Devices). Whole-cell I_h currents were activated by using a voltage step protocol (−50 to −120 mV, 10 mV/step, 5 s or 10 s, V_{hold}: −50 mV). Liquid junction potentials were calculated using the software Junction Potential Calculator (Clampex 9, Molecular Devices), and corrected offline (Ying and Goldstein, 2005). Analysis of I_h currents was performed with Clampfit 10.2 (Molecular Devices) and Sigmaplot 8.0 (Systat). Steady-state activation curves were determined from the amplitude of the tail current measured at −50 mV as previously described (Ying et al., 2006).

Normalized tail current values were plotted as a function of the test voltage and fit with the Boltzmann function. For analysis of activation kinetics, the first 1.5 s of a steady-state current trace (obtained at −120 mV) was fit using a single exponential function to determine the time constant of activation (τ_{act}) (Frère et al., 2004), while the first 2 s of a tail current trace (at −50 mV) was fit with a single exponential function to determine the time constant of deactivation (τ_{deact}). A lag of 50–100 ms in the initial phase of the I_h current trace was excluded from each fit.

I_h electrophysiology in neocortical pyramidal neurons

Pyramidal tract (PT) type cortical projection neurons (in layer 5b, with branches to thalamus) of vibrissal motor cortex were retrogradely labeled by injection of fluorescent beads (RetroBeads, Lumafluor) into motor thalamus (ventral lateral nucleus) at postnatal day 21–22, using WT and KO littermates with the experimenter blind to genotype. Two to six days later, coronal brain sections (0.3 mm thick) containing motor cortex were prepared as described previously (Anderson et al., 2010), and fluorescent neurons in layer 5b of the medial agranular cortex were targeted for whole-cell patch clamp recordings at 34°C (Multiclamp 700B amplifier, Axon Instruments). The potassium-based intracellular solution contained (in mM): 128 $KMeSO_3$, 10 HEPES, 1 EGTA, 4 $MgCl_2$, 4 ATP, 0.4 GTP, 10 phosphocreatine, 3 ascorbate, and 0.05 Alexa-488 hydrazide; pH 7.3. Open-source software *Ephus* (Suter et al., 2010) was used for data acquisition. Traces were filtered at 4 KHz, sampled at 10 KHz, and analyzed off-line using custom routines. Bias current was applied as needed to set the resting membrane potential near −70 mV prior to presenting test protocols. Sag was measured as the percentage difference between the peak amplitude of the initial response (0–0.1 sec after step onset) relative to the peak amplitude of the steady state response (0.4–0.5 sec). Input resistance was calculated from the slope of the linear portion of voltage-current relationships. Sub-threshold resonance was calculated from responses to "chirp" current injection (0–20 Hz, over 20 sec; scaled in amplitude to give ∼5 mV response envelope). For each neuron, the voltage response (averaged over 2–5 trials) and the stimulus were Fourier-transformed, and impedance as a function of frequency was then calculated as the magnitude of the ratio of voltage to current, giving an impedance amplitude profile. Resonant frequency was defined as the peak impedance over 1–20 Hz after boxcar-smoothing (0.75 Hz window). To evaluate temporal summation, excitatory synaptic inputs were simulated as alpha functions, each given by: $I(t) = I_{peak}\,(t/\tau)\,e^{(1-t/\tau)}$, with τ = 5 msec. These were injected in trains of 5 at 20 Hz via the patch pipette, with the I_{peak} adjusted to give ∼5 mV responses to the first event in the train. Summation was calculated for each cell as the ratio of the 5th/1st EPSPs based on an average of 4–5 trials.

RTN electrophysiology

WT and KO mice (P30–50) were deeply anesthetized with isoflurane, decapitated, and the whole brain was rapidly dissected into ice-cold sucrose solution containing (in mM): 190 sucrose, 10 NaCl, 2.5 KCl, 25 $NaHCO_3$, 1.25 NaH_2PO_4, 0.5 $CaCl_2$, 7 $MgCl_2$, 25 dextrose; pH 7.4. All solutions were continuously bubbled with 95% O_2/5% CO_2. 240 μm horizontal slices were made using a microtome (Leica) and immediately transferred to a 35°C holding chamber containing ACSF (125 NaCl, 2.5 KCl, 25 $NaHCO_3$, 1.25 NaH_2PO_4, 2 $CaCl_2$, 1 $MgCl_2$, 25 dextrose; pH 7.4). After a 25-minute incubation period, the chamber was allowed

to equilibrate to room temperature for ≥30 minutes before use. In some experiments kynurenic acid (1 mM) was added to the holding chamber to minimize excitotoxicity. For recording, slices were transferred to a custom chamber perfused with oxygenated ACSF at 1–2 mL/min, warmed to 32°C. RTN neurons were visualized on a Zeiss Axioskop with IR-DIC optics using a CCD camera (Hamamatsu). Electrodes (4–6 MΩ) were pulled on a Sutter P87 pipette puller and filled with intracellular solution containing (in mM): 115 K-gluconate, 20 KCl, 10 HEPES, 10 Na-phosphocreatine, 2 Mg-ATP, 0.3 Na-GTP, 0.2% biocytin, pH to 7.3 with KOH. Whole-cell recordings were made with a PC-ONE amplifier (Dagan), filtered at 3 kHz, and digitized at 20 kHz using an InstruTECH ITC16. Data acquisition and analysis was performed in IgorPro 6 (WaveMetrics) using custom macros. A calculated liquid junction potential of 13 mV was compensated prior to approaching each cell. Series resistance was monitored throughout each experiment and cells were discarded if the series resistance exceeded 30 MΩ. For recording I_h, 1 mM Ba^{2+} was added to the bath solution to block a prominent inward-rectifying potassium current expressed in RTN neurons (Rateau and Ropert, 2006; Ying et al., 2007). NaH_2PO_4 was omitted from Ba^{2+}-containing solutions to avoid precipitation. I_h density at −130 mV was obtained by subtracting the instantaneous current (after the capacitive transient) from the steady-state current at the end of a 2 s step and normalizing to cell capacitance. Synaptic stimulation experiments were performed with the $GABA_A$ blocker SR95531 (2 μm) added to the bath solution. A tungsten electrode (0.1 MΩ, World Precision Instruments) was placed in the internal capsule ∼100 μm from the recorded cell. Trains of 5 biphasic stimuli (0.5 ms each) were delivered at 30 Hz using a stimulus isolation unit (World Precision Instruments). Stimulus intensity was adjusted to achieve EPSPs of 3–5 mV before application of ZD7288 and held constant thereafter. At least 3 sweeps were averaged to obtain pre- and post-ZD7288 EPSP amplitudes for each cell. For stimuli that induced action potential firing, the amplitude was measured at 3 ms following the stimulus, corresponding to the approximate time at which subthreshold EPSPs peaked. Because the amplitude of the 1st EPSP increased significantly in some cells following ZD7288 application, measuring the ratio of the 5th/1st EPSPs was not a reliable indicator of the increased excitability that occurred in the presence of ZD7288. Thus, summation is instead reported as the difference between the amplitudes of the 1st and 5th EPSPs for these recordings.

Immunohistochemistry

WT and KO mice (P75–90) were deeply anesthetized with isoflurane and transcardially perfused with cold PBS followed by 4% PFA. Brains were removed and post-fixed in 4% PFA overnight. The next day, 30 μm coronal sections were made on a vibratome (Leica). Antigen retrieval was performed with 10 mM Na-citrate, pH 9.0, for 10 minutes at 80°C prior to blocking in PBS with 5% normal goat serum and 0.03% Triton X-100 for 1 hour. Primary antibodies were diluted in blocking solution and applied overnight at 4°C. Sections were washed 3 times prior to a 1 hour incubation at room temperature in secondary antibody, followed by 3 additional washes in PBS. DAPI was included in the final wash and tissue was then mounted on glass slides with PermaFluor (Thermo Fisher Scientific). Imaging was performed at the Northwestern University Center for Advanced Microscopy. Images were acquired at 20x on a Nikon C2+ confocal microscope using NIS Elements software (Nikon) and analyzed using ImageJ. To enable comparison of WT and KO tissue,

pairs of animals were processed simultaneously, images for each genotype were acquired with identical settings and are presented with identical look up tables. Primary antibodies used were mouse anti-CC1 (Millipore), mouse anti-parvalbumin (Millipore), and custom rabbit anti-HCN2 and guinea pig anti-TRIP8b (Lewis et al., 2009). All secondary antibodies were purchased from Invitrogen.

Statistics

Data are represented as mean ± SEM unless stated otherwise. Statistical comparisons were evaluated using Student's t-test for 2 groups or one-way ANOVA with Tukey HSD test for pair-wise comparisons among 3 or more groups, unless stated otherwise.

Results

TRIP8b KO mice exhibit spontaneous SWDs

Although we did not observe overt tonic-clonic seizures in our initial characterization of TRIP8b KO mice (Lewis et al., 2011), we suspected that a reduction of HCN channel function in these mice could cause an absence epilepsy phenotype similar to that seen in mice lacking HCN2. Video-EEG recordings revealed that TRIP8b KO mice have spontaneous SWDs (average 5.9 per hour, range 2.2 – 9.4; n = 6 mice) with an average frequency of 5.3 ± 1.7 Hz and an average duration of 1.7 ± 1.0 seconds (mean ± SD; 537 SWDs analyzed) (Fig. 1). SWDs were frequently observed in clusters preceding sleep onset or during brief periods of wakefulness between epochs of sleep (Fig. 1*C*), similar to WAG/Rij rats (Drinkenburg et al., 1991) and many human patients with absence epilepsy (Halász et al., 2002). SWDs were often associated with behavioral arrest (Movie 1), although like human absence epilepsy a clear behavioral response was not always observed (Blumenfeld, 2005; Berman et al., 2010). No SWDs were observed in wild-type (WT) littermates (n = 3 mice, 20 hours analyzed). These data suggest that TRIP8b KO mice may be a novel model for human absence epilepsy, recapitulating both behavioral and electrographic aspects of the disorder. Interestingly, SWDs occurred much less frequently in TRIP8b KO mice than previously observed in HCN2 KO mice (Ludwig et al., 2003) and *apathetic* mice, which harbor a spontaneous mutation in the *Hcn2* gene and lack HCN2 expression (Chung et al., 2009) (see Discussion).

Pharmacological responses of SWDs in TRIP8b KO mice are typical of absence seizures

Human patients and rodent models of absence seizures share a unique pharmacology such that SWDs are suppressed by the calcium channel blocker ethosuximide (Gören and Onat, 2007) and exacerbated by the sodium channel antagonist carbamazepine (Snead and Hosey, 1985). In TRIP8b KO mice, ethosuximide (200 mg/kg) completely suppressed SWDs (Fig. *2A*). Conversely, SWDs were exacerbated by administration of carbamazepine (20 mg/kg), increasing both the number and duration of seizures over an 80-minute recording period post-injection (Fig. *2B–D*). We also tested the susceptibility of TRIP8b KO mice to y-butyrolactone (GBL, 100 mg/kg), which induces absence seizures in a variety of species with similar characteristics to those seen in human patients (Snead, 1991). Latency to onset of SWDs in TRIP8b KO mice was significantly decreased when compared to WT littermates (Fig. 2*E, F*). Furthermore, the total number of SWDs during a 90-minute observation period

following GBL administration was higher in TRIP8b KO mice than in WT (Fig. 2*G*). Taken together, these data suggest that loss of TRIP8b increases susceptibility to both spontaneous and chemically-induced absence seizures.

TRIP8b KO mice do not exhibit motor deficits or sinus dysrhythmia

Motor deficits, particularly cerebellar ataxia, are common to many mouse models of absence epilepsy involving alterations in voltage-gated ion channels (examples include *tottering, lethargic, stargazer, apathetic*; Noebels and Sidman, 1979; Hosford et al., 1992; Letts et al., 1998; Chung et al., 2009; reviewed in Crunelli and Leresche, 2002). Therefore, we assessed TRIP8b KO mice for motor impairment using both fixed-speed and accelerating rotarod tests. Comparison of TRIP8b KO mice, WT littermates, and *apathetic* mice revealed that TRIP8b KO mice performed similarly to WT littermates, while ataxic *apathetic* mice lacking HCN2 expression were completely unable to perform either task (Fig. 3*A*). More subtle motor impairments associated with gait abnormalities were assessed using the DigiGait system (Hampton et al., 2004), which revealed no differences in stride length or stance width between TRIP8b KO mice and WT littermates (Fig. 3*B, C*).

In addition to its multiple functions in the nervous system, I_h also plays a prominent role in pacemaking in the heart, where it contributes to diastolic depolarization in sinoatrial node cells (Baruscotti et al., 2010). Mice lacking HCN2 exhibit sinus dysrhythmia with high variability of the time between successive beats (referred to as RR interval; Ludwig et al., 2003), as shown in Figure 3*D–F* for *apathetic* mice. In contrast, ECG recordings from WT and TRIP8b KO mice demonstrated similar and consistent RR intervals. Additionally, there were no differences in PQ, QRS, and QT intervals nor PQRST morphology between WT and TRIP8b KO mice (data not shown). Normal cardiac rhythm in TRIP8b KO mice is consistent with prior observations that TRIP8b is not expressed in the heart (Amery et al., 2001; Santoro et al., 2004).

Deletion of TRIP8b reduces HCN channel subunit expression in the thalamus and cortex

Reductions in HCN channel function in the cortex and thalamus have been associated with epileptogenesis in several rodent models of absence epilepsy (Ludwig et al., 2003; Strauss et al., 2004; Schridde et al., 2006; Kole et al., 2007; Chung et al., 2009). In light of our previous finding that HCN subunit protein expression is decreased in the hippocampus of TRIP8b KO mice (Lewis et al., 2011), we asked whether the absence epilepsy phenotype observed in TRIP8b KO mice could result from a similar reduction of HCN channels in the thalamus and cortex. Western blotting revealed that TRIP8b KO mice have a 30–50% decrease in protein levels for all HCN channel subunits (HCN1-4) in both regions when compared to WT mice (Fig. 4*A*). Furthermore, using a biotinylation assay to specifically label surface protein, we found an additional 50% reduction in the surface expression of HCN1 and HCN2 in thalamic tissue of TRIP8b KO mice (Fig. 4*B*). Surface expression of GluR1 was measured as a control and did not differ between genotypes. Thus, similar to its role in the hippocampus, TRIP8b appears to be critical for stabilizing and trafficking cortical and thalamic HCN channels.

Reduced I_h and enhanced cAMP responsiveness in thalamocortical neurons of TRIP8b KO mice

To directly assess the functional effects of TRIP8b deletion within the thalamocortical network, we next performed electrophysiological recordings of TC neurons in the ventrobasal (VB) nucleus. Large I_h currents were present in WT VB neurons during hyperpolarizing voltage steps, with dramatically reduced currents in TRIP8b KO neurons (Fig. 5*A*; recorded in "I_h-isolation" solution, see Methods). Comparison of I_h density at −130 mV revealed a 72% reduction in the maximal steady-state current recorded from TRIP8b KO mice (Fig. 5*B*).

HCN2 and HCN4 are the predominant isoforms expressed in VB neurons (Abbas et al., 2006; Ying et al., 2007), and these subunits are particularly responsive to cAMP, exhibiting depolarizing shifts of nearly 20 mV (Chen et al., 2001; Viscomi et al., 2001). Interaction of TRIP8b with the cyclic nucleotide binding domain of HCN channels antagonizes the effect of cAMP *in vitro* (Zolles et al., 2009; Santoro et al., 2011; Hu et al., 2013), but this interaction has never been examined for endogenous neuronal channels. The abundance of cAMP-sensitive HCN channel subunits expressed in VB neurons thus provides an excellent opportunity to study the influence of native TRIP8b on I_h gating properties. Inclusion of the non-hydrolysable cAMP analog 8-Br-cAMP (5 μM) in the recording pipette increased current density by 78% in TRIP8b KO neurons, as compared to 39% in WT neurons (Fig. 5*C, D*). The half-activation voltage ($V_{1/2}$), obtained from Boltzmann fits of the normalized tail currents, was comparable in both genotypes in the absence of exogenous cAMP (Fig. 5*E*). However, TRIP8b KO neurons were significantly more sensitive to cAMP, exhibiting a shift in $V_{1/2}$ of 15.6 ± 1.2 mV compared with 8.0 ± 0.5 mV for WT recordings ($p < 0.001$). Thus, endogenous TRIP8b constrains the effect of cAMP on I_h activation in VB neurons, as was predicted by *in vitro* experiments involving TRIP8b overexpression in cultured hippocampal neurons (Zolles et al., 2009) and oocytes (Santoro et al., 2011; Hu et al., 2013).

In addition to affecting maximal current and $V_{1/2}$, cAMP also accelerates the rate of HCN channel activation and slows the rate of deactivation (Wainger et al., 2001). Similar to our observations of $V_{1/2}$, the time constant of I_h activation was comparable in both genotypes in the absence of exogenous cAMP, and intracellular application of 8-Br-cAMP had a greater accelerating effect in TRIP8b KO neurons than WT neurons (Fig. 6*A, B*). In contrast, deletion of TRIP8b markedly slowed I_h deactivation in the absence of cAMP, increasing the time constant of tail current decay by 175% (Fig. 6*C, D*). Inclusion of 8-Br-cAMP in the recording pipette prolonged I_h deactivation in both WT and TRIP8b KO neurons. Together, these results establish TRIP8b as an important regulatory subunit of native HCN channels in VB neurons, modulating current density, channel gating, and cAMP responsiveness.

I_h-dependent properties are altered in cortical layer 5b neurons of TRIP8b KO mice

Although the 2–4 Hz rhythm underlying SWDs is thought to be generated in the thalamus (Huguenard and McCormick, 2007), existing evidence suggests that aberrant activity initiates in deep layers of the cortex (Meeren et al., 2002; Polack et al., 2007) Interestingly, Kole et al. (2007) found a developmental reduction in I_h in layer 5 pyramidal neurons that occurs concomitant with seizure onset in a rat model of heritable absence epilepsy. Reduced

I_h can strongly increase the excitability of these cells (Kole et al., 2007; Sheets et al., 2011; Santello and Nevian, 2015; although see Harnett et al., 2015), suggesting a potential causative role in the development of absence seizures.

I_h is highly expressed (as is mRNA for HCN1 and TRIP8b) in pyramidal tract (PT) neurons, a subset of layer 5b neurons that project to the spinal cord and other subcortical targets (including thalamus). In contrast, another class of layer 5b neurons that project within the telencephalon (and not to the thalamus) have barely detectible levels of I_h (Sheets et al., 2011; Shepherd, 2013; Harris and Shepherd, 2015). Thus, to determine if deletion of TRIP8b affects the intrinsic properties of thalamically projecting cortical neurons, we recorded specifically from PT neurons in the vibrissal motor cortex by injecting fluorescent retrograde tracers into the motor thalamus (see Materials and Methods). Due to the preferential trafficking of HCN channels to the distal dendrites of these large pyramidal neurons (Berger et al., 2001; Lörincz et al., 2002), electrotonically distant from the recording electrode, somatic voltage clamp experiments are not a reliable means of quantifying I_h (Williams and Mitchell, 2008). Nevertheless, the presence of I_h imparts several characteristic properties that can be measured at the soma under current-clamp conditions. In response to hyperpolarizing steps of current injection, neurons from WT mice showed prominent membrane potential sag, reflecting the slow activation of HCN channels (Fig. 7*A–C*). In contrast, neurons from TRIP8b KO mice showed no sag, implying a dramatic reduction in I_h. Input resistance was also 33% higher in TRIP8b KO neurons (WT 107.6 ± 19.1 MΩ, $n = 11$; KO 143.1 ± 12.2 MΩ, $n = 9$; $p < 0.05$), consistent with a reduction in I_h. Because I_h activates near resting membrane potentials, subthreshold oscillatory inputs generate resonance in the theta frequency range when I_h is present, due to coherence of the input with the kinetics of HCN channel gating (Hutcheon and Yarom, 2000; Sheets et al., 2011). In response to a chirp stimulus (frequency-swept sinusoidal current injection, 0–20 Hz over 20 s), neurons from WT mice showed prominent resonance near 4–5 Hz. In contrast, neurons from TRIP8b KO mice displayed no resonance and a steadily declining impedance amplitude profile (Fig. 7*D–F*). I_h is also known to reduce temporal summation of synaptic inputs by acting as a leak conductance in the dendrites (Magee, 1998). We examined this property by injecting short trains of EPSC-like current waveforms via the patch pipette (Fig. 7*G–I*). In response to trains of five inputs at 20 Hz, neurons from WT mice showed a characteristic lack of summation consistent with high I_h expression. Surprisingly, although neurons from TRIP8b KO mice showed a trend toward increased temporal summation, the effect was not significant ($p = 0.10$) and was much less than previously observed in hippocampal pyramidal neurons of TRIP8b KO mice (Lewis et al., 2011) and layer 5 neurons in rats after pharmacological blockade of I_h (Williams and Stuart, 2000). Additionally, resting membrane potential did not differ between groups (WT −72.4 ± 1.5 mV, n = 11 vs. KO −72.4 ± 2.7 mV, n = 9), in contrast to the hyperpolarized resting potential expected in the absence of I_h. These observations may reflect the induction of compensatory changes in other conductances, as has been observed in HCN1 KO mice (Chen et al., 2010). Nevertheless, the robust decrease in sag and resonance, which are more specific measures of HCN channel function, indicate that deletion of TRIP8b significantly reduces I_h in these cortical projection neurons.

I_h is unaltered in RTN neurons of TRIP8b KO mice

Given the large reductions in I_h we observed in both the cortex and thalamus of TRIP8b KO mice, it is somewhat surprising that these mice display only a mild absence epilepsy phenotype compared to mice lacking HCN2, which have much more frequent seizures (Ludwig et al., 2003; Chung et al., 2009). We hypothesized that this discrepancy could result from differences in RTN function between these strains. The RTN is a thin shell of GABAergic neurons overlying the dorsolateral thalamus that is reciprocally connected to TC neurons in various thalamic nuclei, and also receives strong excitatory inputs from the cortex (Golshani et al., 2001). Output from the RTN can elicit rebound bursts in TC neurons, which feed back to both the cortex and RTN during SWDs to generate repetitive bursts of activity throughout the thalamocortical network (Huguenard and McCormick, 2007).

A previous study identified a crucial role for HCN2 in dampening cortical input onto RTN neurons (Ying et al., 2007). We reasoned that loss of TRIP8b might not affect HCN2 function in RTN neurons if TRIP8b is not normally expressed in these cells. Indeed, on immunohistochemical staining of WT tissue we found that the parvalbumin-positive RTN neurons lacked TRIP8b staining (Fig. 8*A, B*). Interestingly, however, smaller TRIP8b-positive cells were present throughout the RTN. In light of previous reports that TRIP8b and HCN2 are expressed in oligodendrocytes (Notomi and Shigemoto, 2004; Piskorowski et al., 2011), we performed additional immunostaining experiments against the oligodendrocyte marker CC1. As shown in Figure 8*C, D*, the TRIP8b–positive cells in the RTN also express CC1, suggesting TRIP8b is expressed in a subset of oligodendrocytes. Staining for HCN2 also intensely labeled CC1-positive somata in addition to diffusely staining the neuropil. TRIP8b KO tissue did not display any TRIP8b staining, confirming the specificity of our custom antibody. We also found a significant reduction in HCN2 signal intensity in neuropil and oligodendrocyte somata of TRIP8b KO mice (Fig. 8*B, D*), suggesting TRIP8b may play a similar role in stabilizing HCN channels in oligodendrocytes as it does in neurons.

Although the apparent lack of TRIP8b coexpression in parvalbumin-positive RTN neurons supports our hypothesis that TRIP8b is not expressed in these cells, we sought to quantitatively evaluate whether HCN channel function was indeed preserved in RTN neurons using electrophysiological recordings. As has been reported previously (Rateau and Ropert, 2006; Ying et al., 2007), little or no I_h was detectible under standard recording conditions due to the distal, postsynaptic localization of HCN2. However, addition of 1 mM Ba^{2+} to the bath solution to block potassium leak conductances uncovered clear I_h currents in response to hyperpolarizing voltage steps in a subset of RTN neurons (9 of 14 WT cells; 8 of 14 KO cells; Fig. 9*A*). There was no significant difference in I_h density between WT and TRIP8b KO neurons (Fig. 9*B*). To determine whether loss of TRIP8b affects the response of RTN neurons to excitatory inputs, we elicited trains of EPSPs via a stimulating electrode placed in the internal capsule (5 EPSPs at 30 Hz; Fig. 9*C–E*). In the presence of standard ACSF (supplemented with 2 μM SR95531 to block $GABA_A$ receptors), successive EPSPs displayed only modest summation in both genotypes. Bath application of the HCN channel blocker ZD7288 (10 μM) produced a dramatic increase in summation, often sufficient to induce action potential firing by the 4th or 5th EPSP. The response to ZD7288 was comparable in both genotypes, further suggesting that TRIP8b is not required for HCN

channel function in RTN neurons. As with our measurements of I_h, not all RTN neurons exhibited increased excitability after ZD7288 application (3 of 7 WT cells, 3 of 5 KO cells). Thus, it may be that only a subset of RTN neurons express HCN channels. Indeed, numerous studies have identified functional heterogeneity within different RTN populations (Brunton and Charpak, 1997; Lee et al., 2007), including recent findings of distinct subnetworks of RTN cells involved in different attentional states (Halassa et al., 2014; Ahrens et al., 2015).

Discussion

The goal of this study was to characterize the effects of deletion of the HCN channel auxiliary subunit TRIP8b in the mouse thalamus and cortex, focusing on electrophysiological changes and their role in promoting absence epilepsy. We identified spontaneous SWDs in TRIP8b KO mice, occurring at a considerably lower frequency than in other genetic mouse models including HCN2-deficient mice (Ludwig et al., 2003; Chung et al., 2009). Examination of each node of the thalamocortical circuit demonstrated significant reductions in I_h in cortical PT neurons and thalamic VB neurons, but no effect in RTN neurons. TRIP8b KO mice do not have additional neurological phenotypes such as ataxia, and were found to have only minor behavioral changes across a broad range of tests in a previous study (Lewis et al., 2011) despite widespread expression of TRIP8b throughout the brain (Lewis et al., 2009), suggesting that the thalamocortical network is particularly sensitive to changes in I_h.

Function of TRIP8b in TC neurons

Previous work in our lab and others has established TRIP8b as an important auxiliary subunit of HCN channels that is critical for normal channel trafficking in the hippocampus (Lewis et al., 2011; Piskorowski et al., 2011; Wilkars et al., 2012). However, the contribution of TRIP8b to HCN channel function in other brain regions remains largely unexplored. Our current findings provide the first examination of how TRIP8b regulates I_h in the thalamus, demonstrating a similar role in stabilizing HCN protein levels and enhancing surface expression in TC neurons. The large, highly cAMP-responsive current expressed in these cells enabled us to make a detailed examination of the interaction between TRIP8b and cAMP in modulating HCN channel gating. Our data agree with a proposed cyclic allosteric model of TRIP8b and cAMP binding based on prior studies in oocytes (Santoro et al., 2009; Zolles et al., 2009; Hu et al., 2013), and for the first time demonstrate this effect in natively expressed channels in brain slices. In this model, TRIP8b stabilizes the closed state of the channel and cAMP stabilizes the open state. This antagonistic relationship explains the larger cAMP-induced shift in $V_{1/2}$, activation kinetics, and maximum current following loss of TRIP8b. The dynamic interplay between TRIP8b and cAMP likely contributes to the modulation of I_h in TC neurons during different behavioral states (McCormick and Bal, 1997), and may also have important physiological functions in other brain regions.

Role of I_h in thalamocortical networks and absence seizures

We initially suspected that TRIP8b KO mice may exhibit absence seizures based on our experience with the *apathetic* HCN2 mutant line (Chung et al., 2009). Compared with *apathetic* mice, however, it is clear that the TRIP8b KO constitutes only a mild absence phenotype. Whereas we observed an average of 6 SWDs per hour here, *apathetic* mice average ∼250. Although strain differences have been shown to influence susceptibility to SWDs (Tokuda et al., 2009) and could account for some of the difference in SWD frequency between TRIP8b KO and *apathetic* mice, targeted HCN2 KO mice with the same genetic background as TRIP8b KO mice (C57BL/6) have 10-fold more frequent SWDs than TRIP8b KO mice (Ludwig et al., 2003; quantified as 3% of the light-phase EEG, versus 0.3% in TRIP8b KO mice). Thus, while background strain may modulate seizure frequency, it is unlikely to fully explain the dramatic difference between mice lacking TRIP8b versus HCN2. It is perhaps not surprising that loss of a channel auxiliary subunit might result in a less severe phenotype than loss of the pore-forming protein. However, deletion of TRIP8b reduced I_h in TC neurons nearly as much as deletion of HCN2 (72% vs. 79%; Ludwig et al., 2003). The enhanced sensitivity to cAMP in TRIP8b KO mice may partially compensate for this deficit, particularly during states of vigilance when cAMP signaling is high (McCormick, 1992). This idea is consistent with our observation that SWDs occurred preferentially surrounding epochs of sleep. Nevertheless, even with saturating cAMP concentrations I_h is reduced by over 50% in TRIP8b KO TC neurons. Furthermore, I_h was found to be increased rather than decreased in TC neurons in two different rat models of absence epilepsy when compared to non-epileptic strains (Kanyshkova et al., 2012; Cain et al., 2014). Thus, the amount of I_h in these cells is poorly correlated with seizure burden, and cannot explain the dramatic difference in SWD rate between TRIP8b KO and HCN2 null mice.

Differences in cortical function are also unlikely to account for variability in SWDs between these mice. HCN2 is expressed at much lower levels in neocortical pyramidal neurons, where HCN1 accounts for the majority of I_h (Notomi and Shigemoto, 2004; Chen et al., 2009; Sheets et al., 2011). In the HCN2 KO mice, Ludwig *et al*. found only a 30% reduction in I_h in CA1 pyramidal neurons, which is likely to be comparable in the neocortex (Chen et al., 2009). In contrast, TRIP8b KO mice have undetectable measures of I_h in thalamic-projecting layer 5b neurons. Because I_h has a well established anti-excitatory influence in many classes of pyramidal neurons (Magee, 1998; Strauss et al., 2004; Kole et al., 2007; Tsay et al., 2007; Sheets et al., 2011), cortical circuits are likely to be more excitable in TRIP8b KO mice relative to HCN2 null mice.

The frequent absence seizures in HCN2 KO mice were initially attributed to an increased propensity for burst firing in TC neurons, resulting from membrane hyperpolarization and subsequent relief of T-type Ca^{2+} channel inactivation (Ludwig et al., 2003). However, the comparison with TRIP8b KO mice above suggests that this mechanism is unlikely to be the major driver of SWD initiation in the HCN2 KO. Later work identified an important role for HCN2 in dampening excitatory inputs onto RTN neurons (Ying et al., 2007). Colocalization with AMPA receptors (specifically GluR4) within dendritic spines provides a shunt conductance such that loss or blockade of HCN2 dramatically increases EPSP amplitude and

summation, with a concomitant increase in IPSP output to TC neurons. Unlike in pyramidal neurons, this dendritic trafficking of HCN2 does not appear to be TRIP8b-dependent, as we were unable to detect TRIP8b staining in parvalbumin-expressing neurons, and I_h was undiminished in RTN neurons of TRIP8b KO mice. Furthermore, we found that ZD7288 enhanced EPSPs to a similar extent in TRIP8b KO and WT mice, providing additional evidence that HCN channel function is intact in RTN neurons.

Taken together, the considerations above suggest that I_h in RTN neurons is critical for stabilizing thalamocortical network activity, even more so than the much larger I_h currents found in TC neurons. This model is consistent with a large body of work demonstrating the importance of the RTN in synchronizing large populations of TC neurons during SWDs (Meeren et al., 2009; Zaman et al., 2011; Lacey et al., 2012; reviewed in Huguenard and McCormick, 2007). In TRIP8b KO mice, preserved I_h in RTN neurons seems to largely compensate for significantly decreased I_h in cortical and TC neurons, resulting in far fewer SWDs compared to mice lacking HCN2. The sparse SWDs that do occur likely result from hyperexcitability within cortical circuits, given that the cortex is the suspected site of SWD initiation (Meeren et al., 2002; Polack et al., 2007; Leresche et al., 2012). Augmented cortical volleys in TRIP8b KO mice may be able synchronously recruit large numbers of RTN neurons, even when the RTN itself is not hyperexcitable. Indeed, a similar pattern of activity has been demonstrated in thalamic slice preparations (Bal et al., 2000; Blumenfeld and McCormick, 2000) and in modeling studies of thalamocortical networks (Destexhe et al., 1998). Alternatively, cortical inputs may bypass the RTN entirely and directly excite TC neurons to initiate SWDs, as observed in GRIA4 KO mice (Paz et al., 2011). Region- and cell-type-specific deletions of TRIP8b may be informative in elucidating the precise sequence of activity leading to SWDs in TRIP8b KO mice.

Relevance to absence epilepsy in humans

In summary, we have identified the TRIP8b KO mouse as a novel model of absence epilepsy, without additional neurological impairments such as ataxia that are common in other mouse models. The rate of SWDs in TRIP8b KO mice (~6 per hour) is significantly less than most other genetic rodent models, including *apathetic* and HCN2 KO mice, but is actually more representative of typical human patients with childhood absence epilepsy (for example, Dlugos et al., 2013 report a median of 5 seizures per hour in a cohort of 445 patients). Although TRIP8b has not been associated with any cases of human epilepsy to date, a loss-of-function mutation in HCN2 was identified in a patient with severe generalized epilepsy featuring absence and tonic-clonic seizures (DiFrancesco et al., 2011) The parallels between this patient and mice lacking HCN2 suggest that alterations in I_h may cause neurological disease in humans similar to that observed in mice.

One notable discrepancy between humans and these mouse models is in seizure duration, which frequently exceeds 10 seconds in humans but was almost never longer than 3 seconds in either TRIP8b KO or *apathetic* mice (Chung et al., 2009). Although extensive work has been devoted to understanding the mechanisms of SWD initiation, generalization, and rhythmicity, comparatively little is known about the determinants of seizure duration and termination. Interestingly, models of sleep spindles, which may also be relevant to absence

seizures (Beenhakker and Huguenard, 2009), incorporate a slowly developing, persistent activation of I_h in TC neurons that terminates spindle oscillations (Lüthi et al., 1998). However, if this mechanism is important for SWD termination, our data suggest it does not rely on TRIP8b or HCN2. Further investigation of this issue may provide important new insights into the pathogenesis of absence seizures.

Supplementary Material

Refer to Web version on PubMed Central for supplementary material.

Acknowledgements

This research was supported by National Institutes of Health (NIH) grants NS064757 (A.S.L.), NS067193 and NS059934 (D.M.C.), NS061963 (G.M.G.S.), and MH048432 (D.J.), as well as by a Brain Research Foundation Seed Grant (D.M.C.) and the Dept. of Anesthesiology, Weill Cornell Medical College (P.A.G.). Imaging work was performed at the Northwestern University Center for Advanced Microscopy supported by NCI CCSG P30 CA060553 awarded to the Robert H. Lurie Comprehensive Cancer Center. We thank Quratul-Ain Ismail and Andrey Popov for technical support, and Daniel Fisher for comments on the manuscript.

Abbreviations

HCN	hyperpolarization-activated cyclic-nucleotide-gated
RTN	reticular thalamic nucleus
SWD	spike-wave discharge
TC	thalamocortical
TRIP8b	tetratricopeptide-containing Rab8b-interacting protein

References

Abbas SY, Ying SW, Goldstein PA. Compartmental distribution of hyperpolarization-activated cyclic-nucleotide-gated channel 2 and hyperpolarization-activated cyclic-nucleotide-gated channel 4 in thalamic reticular and thalamocortical relay neurons. Neuroscience. 2006; 141:1811–1825. [PubMed: 16806719]

Ahrens S, Jaramillo S, Yu K, Ghosh S, Hwang G-R, Paik R, Lai C, He M, Huang ZJ, Li B. ErbB4 regulation of a thalamic reticular nucleus circuit for sensory selection. Nature Neuroscience. 2015; 18:104–111. [PubMed: 25501036]

Amery L, Sano H, Mannaerts GP, Snider J, Van Looy J, Fransen M, Van Veldhoven PP. Identification of PEX5p–related novel peroxisome-targeting signal 1 (PTS1)-binding proteins in mammals. Biochem J. 2001; 357:635–646. [PubMed: 11463335]

Anderson CT, Sheets PL, Kiritani T, Shepherd GMG. Sublayer-specific microcircuits of corticospinal and corticostriatal neurons in motor cortex. Nature Neuroscience. 2010; 13:739–744. [PubMed: 20436481]

Avoli M. A brief history on the oscillating roles of thalamus and cortex in absence seizures. Epilepsia. 2012; 53:779–789. [PubMed: 22360294]

Bal T, Debay D, Destexhe A. Cortical feedback controls the frequency and synchrony of oscillations in the visual thalamus. Journal of Neuroscience. 2000; 20:7478–7488. [PubMed: 11007907]

Baruscotti M, Barbuti A, Bucchi A. The cardiac pacemaker current. J Mol Cell Cardiol. 2010; 48:55–64. [PubMed: 19591835]

Beenhakker MP, Huguenard JR. Neurons that fire together also conspire together: is normal sleep circuitry hijacked to generate epilepsy? Neuron. 2009; 62:612–632. [PubMed: 19524522]

Berger T, Larkum ME, Lüscher HR. High I(h) channel density in the distal apical dendrite of layer V pyramidal cells increases bidirectional attenuation of EPSPs. J Neurophysiol. 2001; 85:855–868. [PubMed: 11160518]

Berman R, Negishi M, Vestal M, Spann M, Chung MH, Bai X, Purcaro M, Motelow JE, Danielson N, Dix-Cooper L, Enev M, Novotny EJ, Constable RT, Blumenfeld H. Simultaneous EEG, fMRI, and behavior in typical childhood absence seizures. Epilepsia. 2010; 51:2011–2022. [PubMed: 20608963]

Biel M, Wahl-Schott C, Michalakis S, Zong X. Hyperpolarization-activated cation channels: from genes to function. Physiol Rev. 2009; 89:847–885. [PubMed: 19584315]

Blumenfeld H. Consciousness and epilepsy: why are patients with absence seizures absent? Prog Brain Res. 2005; 150:271–286. [PubMed: 16186030]

Blumenfeld H, McCormick DA. Corticothalamic inputs control the pattern of activity generated in thalamocortical networks. Journal of Neuroscience. 2000; 20:5153–5162. [PubMed: 10864972]

Brunton J, Charpak S. Heterogeneity of cell firing properties and opioid sensitivity in the thalamic reticular nucleus. Neuroscience. 1997; 78:303–307. [PubMed: 9145788]

Budde T, Caputi L, Kanyshkova T, Staak R, Abrahamczik C, Munsch T, Pape H-C. Impaired regulation of thalamic pacemaker channels through an imbalance of subunit expression in absence epilepsy. Journal of Neuroscience. 2005; 25:9871–9882. [PubMed: 16251434]

Cain SM, Tyson JR, Jones KL, Snutch TP. Thalamocortical neurons display suppressed burst-firing due to an enhanced Ih current in a genetic model of absence epilepsy. Pflugers Arch. 2014; 467:1367–1382. [PubMed: 24953239]

Chen S, Wang J, Siegelbaum SA. Properties of hyperpolarization-activated pacemaker current defined by coassembly of HCN1 and HCN2 subunits and basal modulation by cyclic nucleotide. J Gen Physiol. 2001; 117:491–504. [PubMed: 11331358]

Chen X, Shu S, Kennedy DP, Willcox SC, Bayliss DA. Subunit-specific effects of isoflurane on neuronal Ih in HCN1 knockout mice. J Neurophysiol. 2009; 101:129–140. [PubMed: 18971302]

Chen X, Shu S, Schwartz LC, Sun C, Kapur J, Bayliss DA. Homeostatic regulation of synaptic excitability: tonic GABA(A) receptor currents replace I(h) in cortical pyramidal neurons of HCN1 knock-out mice. Journal of Neuroscience. 2010; 30:2611–2622. [PubMed: 20164346]

Chu V, Otero JM, Lopez O, Morgan JP, Amende I, Hampton TG. Method for non-invasively recording electrocardiograms in conscious mice. BMC Physiol. 2001; 1:6. [PubMed: 11476671]

Chung WK, Shin M, Jaramillo TC, Leibel RL, LeDuc CA, Fischer SG, Tzilianos E, Gheith AA, Lewis AS, Chetkovich DM. Absence epilepsy in apathetic, a spontaneous mutant mouse lacking the h channel subunit, HCN2. Neurobiol Dis. 2009; 33:499–508. [PubMed: 19150498]

Crunelli V, Leresche N. Childhood absence epilepsy: genes, channels, neurons and networks. Nat Rev Neurosci. 2002; 3:371–382. [PubMed: 11988776]

Deng H, Xiu X, Song Z. The molecular biology of genetic-based epilepsies. Mol Neurobiol. 2014; 49:352–367. [PubMed: 23934645]

Destexhe A, Contreras D, Steriade M. Mechanisms underlying the synchronizing action of corticothalamic feedback through inhibition of thalamic relay cells. J Neurophysiol. 1998; 79:999–1016. [PubMed: 9463458]

DiFrancesco JC, Barbuti A, Milanesi R, Coco S, Bucchi A, Bottelli G, Ferrarese C, Franceschetti S, Terragni B, Baruscotti M, DiFrancesco D. Recessive loss-of-function mutation in the pacemaker HCN2 channel causing increased neuronal excitability in a patient with idiopathic generalized epilepsy. Journal of Neuroscience. 2011; 31:17327–17337. [PubMed: 22131395]

Dlugos D, Shinnar S, Cnaan A, Hu F, Moshé S, Mizrahi E, Masur D, Sogawa Y, Le Pichon JB, Levine C, Hirtz D, Clark P, Adamson PC, Glauser T. Childhood Absence Epilepsy Study Team. Pretreatment EEG in childhood absence epilepsy: associations with attention and treatment outcome. Neurology. 2013; 81:150–156. [PubMed: 23719147]

Drinkenburg WH, Coenen AM, Vossen JM, van Luijtelaar EL. Spike-wave discharges and sleep-wake states in rats with absence epilepsy. Epilepsy Res. 1991; 9:218–224. [PubMed: 1743184]

Frère SGA, Kuisle M, Lüthi A. Regulation of recombinant and native hyperpolarization-activated cation channels. Mol Neurobiol. 2004; 30:279–305. [PubMed: 15655253]

Glauser TA, Cnaan A, Shinnar S, Hirtz DG, Dlugos D, Masur D, Clark PO, Capparelli EV, Adamson PC. Childhood Absence Epilepsy Study Group. Ethosuximide, valproic acid, and lamotrigine in childhood absence epilepsy. N Engl J Med. 2010; 362:790–799. [PubMed: 20200383]

Golshani P, Liu XB, Jones EG. Differences in quantal amplitude reflect GluR4-subunit number at corticothalamic synapses on two populations of thalamic neurons. Proc Natl Acad Sci USA. 2001; 98:4172–4177. [PubMed: 11274440]

Gören MZ, Onat F. Ethosuximide: from bench to bedside. CNS Drug Rev. 2007; 13:224–239. [PubMed: 17627674]

Halassa MM, Chen Z, Wimmer RD, Brunetti PM, Zhao S, Zikopoulos B, Wang F, Brown EN, Wilson MA. State-dependent architecture of thalamic reticular subnetworks. Cell. 2014; 158:808–821. [PubMed: 25126786]

Halász P, Terzano MG, Parrino L. Spike-wave discharge and the microstructure of sleep-wake continuum in idiopathic generalised epilepsy. Neurophysiol Clin. 2002; 32:38–53. [PubMed: 11915485]

Hampton TG, Kale A, McCue S, Bhagavan HN, Vandongen C. Developmental Changes in the ECG of a Hamster Model of Muscular Dystrophy and Heart Failure. Front Pharmacol. 2012; 3:80. [PubMed: 22629245]

Hampton TG, Stasko MR, Kale A, Amende I, Costa ACS. Gait dynamics in trisomic mice: quantitative neurological traits of Down syndrome. Physiol Behav. 2004; 82:381–389. [PubMed: 15276802]

Harnett MT, Magee JC, Williams SR. Distribution and Function of HCN Channels in the Apical Dendritic Tuft of Neocortical Pyramidal Neurons. Journal of Neuroscience. 2015; 35:1024–1037. [PubMed: 25609619]

Harris KD, Shepherd GMG. The neocortical circuit: themes and variations. Nature Neuroscience. 2015; 18:170–181. [PubMed: 25622573]

Hosford DA, Clark S, Cao Z, Wilson WA, Lin FH, Morrisett RA, Huin A. The role of GABAB receptor activation in absence seizures of lethargic (lh/lh) mice. Science. 1992; 257:398–401. [PubMed: 1321503]

Hu L, Santoro B, Saponaro A, Liu H, Moroni A, Siegelbaum S. Binding of the auxiliary subunit TRIP8b to HCN channels shifts the mode of action of cAMP. J Gen Physiol. 2013; 142:599–612. [PubMed: 24277603]

Huguenard JR, McCormick DA. Thalamic synchrony and dynamic regulation of global forebrain oscillations. Trends Neurosci. 2007; 30:350–356. [PubMed: 17544519]

Hutcheon B, Yarom Y. Resonance, oscillation and the intrinsic frequency preferences of neurons. Trends Neurosci. 2000; 23:216–222. [PubMed: 10782127]

Jallon P, Loiseau P, Loiseau J. Newly diagnosed unprovoked epileptic seizures: presentation at diagnosis in CAROLE study. Coordination Active du Réseau Observatoire Longitudinal de l' Epilepsie. Epilepsia. 2001; 42:464–475. [PubMed: 11440341]

Kanyshkova T, Meuth P, Bista P, Liu Z, Ehling P, Caputi L, Doengi M, Chetkovich DM, Pape H-C, Budde T. Differential regulation of HCN channel isoform expression in thalamic neurons of epileptic and non-epileptic rat strains. Neurobiol Dis. 2012; 45:450–461. [PubMed: 21945537]

Kole MHP, Bräuer AU, Stuart GJ. Inherited cortical HCN1 channel loss amplifies dendritic calcium electrogenesis and burst firing in a rat absence epilepsy model. J Physiol (Lond). 2007; 578:507–525. [PubMed: 17095562]

Lacey CJ, Bryant A, Brill J, Huguenard JR. Enhanced NMDA receptor-dependent thalamic excitation and network oscillations in stargazer mice. Journal of Neuroscience. 2012; 32:11067–11081. [PubMed: 22875939]

Lee S-H, Govindaiah G, Cox CL. Heterogeneity of firing properties among rat thalamic reticular nucleus neurons. J Physiol (Lond). 2007; 582:195–208. [PubMed: 17463035]

Leresche N, Lambert RC, Errington AC, Crunelli V. From sleep spindles of natural sleep to spike and wave discharges of typical absence seizures: is the hypothesis still valid? Pflugers Arch. 2012; 463:201–212. [PubMed: 21861061]

Letts VA, Felix R, Biddlecome GH, Arikkath J, Mahaffey CL, Valenzuela A, Bartlett FS, Mori Y, Campbell KP, Frankel WN. The mouse stargazer gene encodes a neuronal Ca2+-channel gamma subunit. Nat Genet. 1998; 19:340–347. [PubMed: 9697694]

Lewis AS, Schwartz E, Chan CS, Noam Y, Shin M, Wadman WJ, Surmeier DJ, Baram TZ, Macdonald RL, Chetkovich DM. Alternatively spliced isoforms of TRIP8b differentially control h channel trafficking and function. Journal of Neuroscience. 2009; 29:6250–6265. [PubMed: 19439603]

Lewis AS, Vaidya SP, Blaiss CA, Liu Z, Stoub TR, Brager DH, Chen X, Bender RA, Estep CM, Popov AB, Kang CE, Van Veldhoven PP, Bayliss DA, Nicholson DA, Powell CM, Johnston D, Chetkovich DM. Deletion of the hyperpolarization-activated cyclic nucleotide-gated channel auxiliary subunit TRIP8b impairs hippocampal Ih localization and function and promotes antidepressant behavior in mice. Journal of Neuroscience. 2011; 31:7424–7440. [PubMed: 21593326]

Llinás RR, Steriade M. Bursting of thalamic neurons and states of vigilance. J Neurophysiol. 2006; 95:3297–3308. [PubMed: 16554502]

Lörincz A, Notomi T, Tamás G, Shigemoto R, Nusser Z. Polarized and compartment-dependent distribution of HCN1 in pyramidal cell dendrites. Nature Neuroscience. 2002; 5:1185–1193. [PubMed: 12389030]

Ludwig A, Budde T, Stieber J, Moosmang S, Wahl C, Holthoff K, Langebartels A, Wotjak C, Munsch T, Zong X, Feil S, Feil R, Lancel M, Chien KR, Konnerth A, Pape H-C, Biel M, Hofmann F. Absence epilepsy and sinus dysrhythmia in mice lacking the pacemaker channel HCN2. EMBO J. 2003; 22:216–224. [PubMed: 12514127]

Lüthi A, Bal T, McCormick DA. Periodicity of thalamic spindle waves is abolished by ZD7288,a blocker of Ih. J Neurophysiol. 1998; 79:3284–3289. [PubMed: 9636128]

Magee JC. Dendritic hyperpolarization-activated currents modify the integrative properties of hippocampal CA1 pyramidal neurons. J Neurosci. 1998; 18:7613–7624. [PubMed: 9742133]

McCormick DA. Neurotransmitter actions in the thalamus and cerebral cortex and their role in neuromodulation of thalamocortical activity. Prog Neurobiol. 1992; 39:337–388. [PubMed: 1354387]

McCormick DA, Bal T. Sleep and arousal: thalamocortical mechanisms. Annu Rev Neurosci. 1997; 20:185–215. [PubMed: 9056712]

Meeren HKM, Pijn JPM, Van Luijtelaar ELJM, Coenen AML, Lopes da Silva FH. Cortical focus drives widespread corticothalamic networks during spontaneous absence seizures in rats. Journal of Neuroscience. 2002; 22:1480–1495. [PubMed: 11850474]

Meeren HKM, Veening JG, Möderscheim TAE, Coenen AML, van Luijtelaar G. Thalamic lesions in a genetic rat model of absence epilepsy: dissociation between spike-wave discharges and sleep spindles. Exp Neurol. 2009; 217:25–37. [PubMed: 19416679]

Noebels JL, Sidman RL. Inherited epilepsy: spike-wave and focal motor seizures in the mutant mouse tottering. Science. 1979; 204:1334–1336. [PubMed: 572084]

Notomi T, Shigemoto R. Immunohistochemical localization of Ih channel subunits, HCN1-4, in the rat brain. J Comp Neurol. 2004; 471:241–276. [PubMed: 14991560]

Pavone P, Bianchini R, Trifiletti RR, Incorpora G, Pavone A, Parano E. Neuropsychological assessment in children with absence epilepsy. Neurology. 2001; 56:1047–1051. [PubMed: 11320177]

Paz JT, Bryant AS, Peng K, Fenno L, Yizhar O, Frankel WN, Deisseroth K, Huguenard JR. A new mode of corticothalamic transmission revealed in the Gria4(−/−) model of absence epilepsy. Nature Neuroscience. 2011; 14:1167–1173. [PubMed: 21857658]

Piskorowski R, Santoro B, Siegelbaum SA. TRIP8b splice forms act in concert to regulate the localization and expression of HCN1 channels in CA1 pyramidal neurons. Neuron. 2011; 70:495–509. [PubMed: 21555075]

Polack P-O, Guillemain I, Hu E, Deransart C, Depaulis A, Charpier S. Deep layer somatosensory cortical neurons initiate spike-and-wave discharges in a genetic model of absence seizures. Journal of Neuroscience. 2007; 27:6590–6599. [PubMed: 17567820]

Rateau Y, Ropert N. Expression of a functional hyperpolarization-activated current (Ih) in the mouse nucleus reticularis thalami. J Neurophysiol. 2006; 95:3073–3085. [PubMed: 16617177]

Santello M, Nevian T. Dysfunction of Cortical Dendritic Integration in Neuropathic Pain Reversed by Serotoninergic Neuromodulation. Neuron. 2015

Santoro B, Hu L, Liu H, Saponaro A, Pian P, Piskorowski RA, Moroni A, Siegelbaum SA. TRIP8b regulates HCN1 channel trafficking and gating through two distinct C-terminal interaction sites. Journal of Neuroscience. 2011; 31:4074–4086. [PubMed: 21411649]

Santoro B, Piskorowski RA, Pian P, Hu L, Liu H, Siegelbaum SA. TRIP8b splice variants form a family of auxiliary subunits that regulate gating and trafficking of HCN channels in the brain. Neuron. 2009; 62:802–813. [PubMed: 19555649]

Santoro B, Wainger BJ, Siegelbaum SA. Regulation of HCN channel surface expression by a novel C-terminal protein-protein interaction. Journal of Neuroscience. 2004; 24:10750–10762. [PubMed: 15564593]

Schridde U, Strauss U, Bräuer AU, van Luijtelaar G. Environmental manipulations early in development alter seizure activity, Ih and HCN1 protein expression later in life. Eur J Neurosci. 2006; 23:3346–3358. [PubMed: 16820024]

Sheets PL, Suter BA, Kiritani T, Chan CS, Surmeier DJ, Shepherd GMG. Corticospinal-specific HCN expression in mouse motor cortex: I(h)-dependent synaptic integration as a candidate microcircuit mechanism involved in motor control. J Neurophysiol. 2011; 106:2216–2231. [PubMed: 21795621]

Shepherd GMG. Corticostriatal connectivity and its role in disease. Nat Rev Neurosci. 2013; 14:278–291. [PubMed: 23511908]

Shin M, Brager D, Jaramillo TC, Johnston D, Chetkovich DM. Mislocalization of h channel subunits underlies h channelopathy in temporal lobe epilepsy. Neurobiol Dis. 2008; 32:26–36. [PubMed: 18657617]

Shin M, Simkin D, Suyeoka GM, Chetkovich DM. Evaluation of HCN2 abnormalities as a cause of juvenile audiogenic seizures in Black Swiss mice. Brain Res. 2006; 1083:14–20. [PubMed: 16542642]

Snead OC. The gamma-hydroxybutyrate model of absence seizures: correlation of regional brain levels of gamma-hydroxybutyric acid and gamma-butyrolactone with spike wave discharges. Neuropharmacology. 1991; 30:161–167. [PubMed: 2030821]

Snead OC, Hosey LC. Exacerbation of seizures in children by carbamazepine. N Engl J Med. 1985; 313:916–921. [PubMed: 3929090]

Staak R, Pape HC. Contribution of GABA(A) and GABA(B) receptors to thalamic neuronal activity during spontaneous absence seizures in rats. Journal of Neuroscience. 2001; 21:1378–1384. [PubMed: 11160409]

Strauss U, Kole MHP, Bräuer AU, Pahnke J, Bajorat R, Rolfs A, Nitsch R, Deisz RA. An impaired neocortical Ih is associated with enhanced excitability and absence epilepsy. Eur J Neurosci. 2004; 19:3048–3058. [PubMed: 15182313]

Suter BA, O'Connor T, Iyer V, Petreanu LT, Hooks BM, Kiritani T, Svoboda K, Shepherd GMG. Ephus: multipurpose data acquisition software for neuroscience experiments. Front Neural Circuits. 2010; 4:100. [PubMed: 21960959]

Tokuda S, Beyer BJ, Frankel WN. Genetic complexity of absence seizures in substrains of C3H mice. Genes Brain Behav. 2009; 8:283–289. [PubMed: 19170754]

Tsay D, Dudman JT, Siegelbaum SA. HCN1 channels constrain synaptically evoked Ca2+ spikes in distal dendrites of CA1 pyramidal neurons. Neuron. 2007; 56:1076–1089. [PubMed: 18093528]

Viscomi C, Altomare C, Bucchi A, Camatini E, Baruscotti M, Moroni A, DiFrancesco D. C terminus-mediated control of voltage and cAMP gating of hyperpolarization-activated cyclic nucleotide-gated channels. J Biol Chem. 2001; 276:29930–29934. [PubMed: 11397812]

Wainger BJ, DeGennaro M, Santoro B, Siegelbaum SA, Tibbs GR. Molecular mechanism of cAMP modulation of HCN pacemaker channels. Nature. 2001; 411:805–810. [PubMed: 11459060]

Wilkars W, Liu Z, Lewis AS, Stoub TR, Ramos EM, Brandt N, Nicholson DA, Chetkovich DM, Bender RA. Regulation of Axonal HCN1 Trafficking in Perforant Path Involves Expression of Specific TRIP8b Isoforms. PLoS ONE. 2012; 7:e32181. [PubMed: 22363812]

Williams SR, Mitchell SJ. Direct measurement of somatic voltage clamp errors in central neurons. Nature Neuroscience. 2008; 11:790–798. [PubMed: 18552844]

Williams SR, Stuart GJ. Site independence of EPSP time course is mediated by dendritic I(h) in neocortical pyramidal neurons. J Neurophysiol. 2000; 83:3177–3182. [PubMed: 10805715]

Ying S-W, Abbas SY, Harrison NL, Goldstein PA. Propofol block of I(h) contributes to the suppression of neuronal excitability and rhythmic burst firing in thalamocortical neurons. Eur J Neurosci. 2006; 23:465–480. [PubMed: 16420453]

Ying S-W, Goldstein PA. Propofol-block of SK channels in reticular thalamic neurons enhances GABAergic inhibition in relay neurons. J Neurophysiol. 2005; 93:1935–1948. [PubMed: 15563549]

Ying S-W, Jia F, Abbas SY, Hofmann F, Ludwig A, Goldstein PA. Dendritic HCN2 channels constrain glutamate-driven excitability in reticular thalamic neurons. Journal of Neuroscience. 2007; 27:8719–8732. [PubMed: 17687049]

Zaman T, Lee K, Park C, Paydar A, Choi JH, Cheong E, Lee CJ, Shin H-S. Cav2.3 channels are critical for oscillatory burst discharges in the reticular thalamus and absence epilepsy. Neuron. 2011; 70:95–108. [PubMed: 21482359]

Zolles G, Wenzel D, Bildl W, Schulte U, Hofmann A, Müller CS, Thumfart J-O, Vlachos A, Deller T, Pfeifer A, Fleischmann BK, Roeper J, Fakler B, Klöcker N. Association with the auxiliary subunit PEX5R/Trip8b controls responsiveness of HCN channels to cAMP and adrenergic stimulation. Neuron. 2009; 62:814–825. [PubMed: 19555650]

Highlights

- TRIP8b is an auxiliary subunit of HCN channels that regulates neuronal excitability.
- We noted spontaneous absence seizures during EEG recordings of TRIP8b knockout mice.
- We found reduced HCN channel function (I_h) in neurons of the cortex and thalamus.
- Normal I_h in the reticular thalamic nucleus may limit seizure severity in these mice.

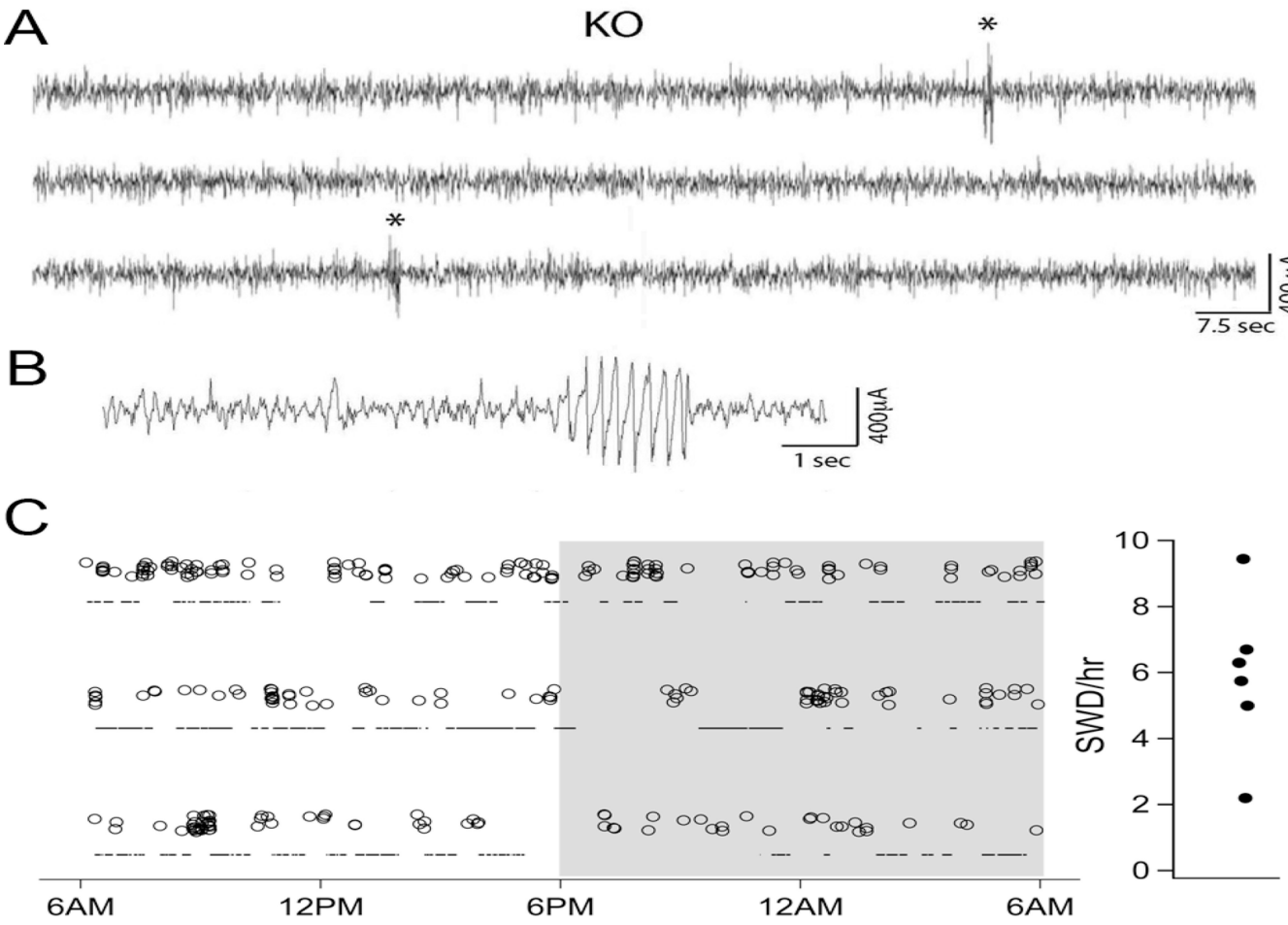

Figure 1.

TRIP8b KO mice exhibit spontaneous SWDs. **A**, Representative EEG recording from a freely moving TRIP8b KO mouse (12 min continuous trace). Asterisks denote SWDs. **B**, Expanded trace demonstrating SWD morphology. **C**, Distribution of SWDs over a 24-hr recording period in 3 KO mice (left), and mean number of SWDs/hr during the awake-phase EEG for each of 6 KO mice recorded (right). Bars under each SWD plot indicate periods of slow-wave sleep.

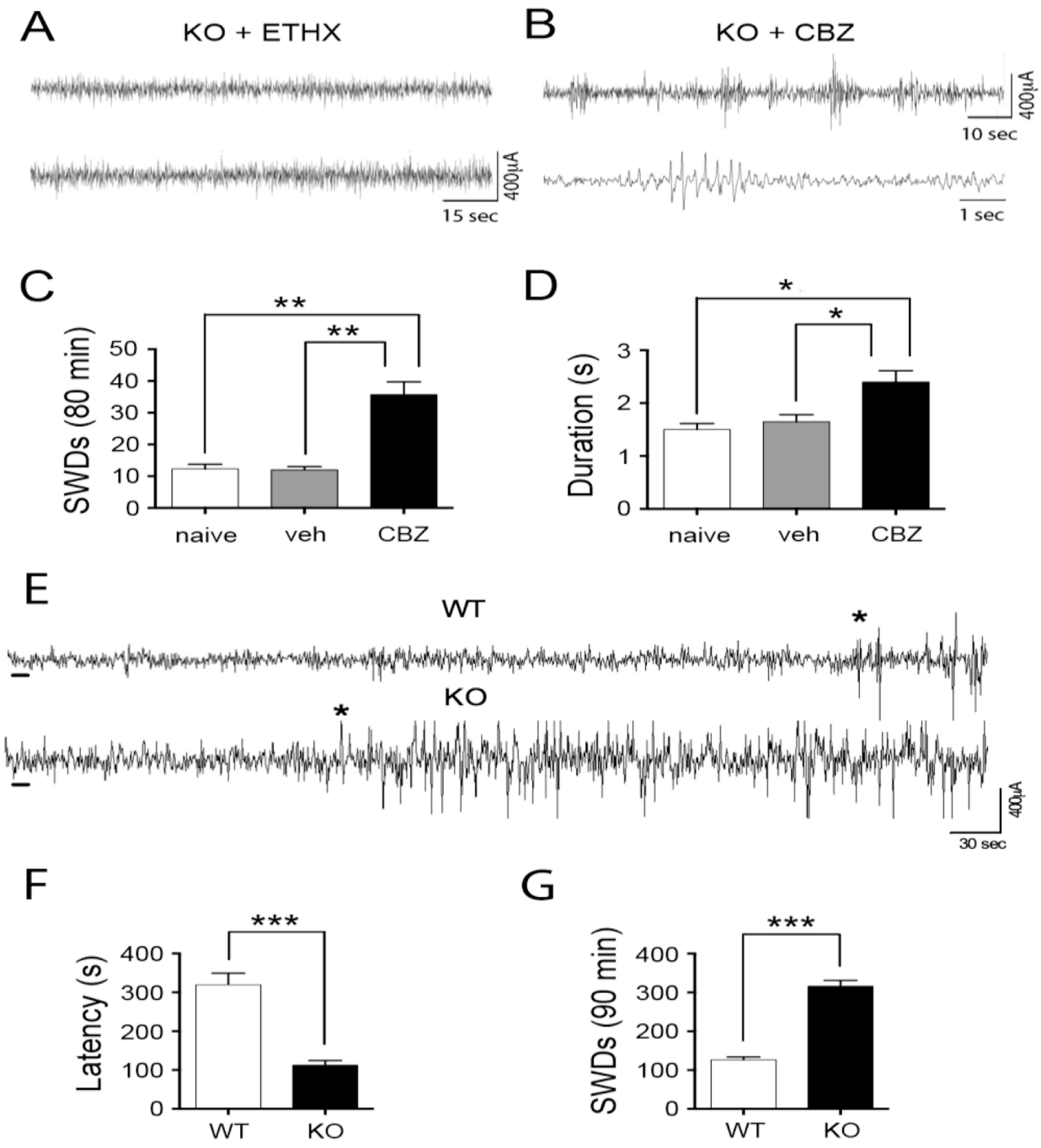

Figure 2.

SWDs in TRIP8b KO mice exhibit absence-like pharmacology. **A**, Representative trace demonstrating that SWDs in the TRIP8b KO mouse were completely suppressed following administration of ethosuximide (ETHX, n = 6 KO mice recorded). **B**, Representative EEG traces from a TRIP8b KO mouse after administration of carbamazepine (CBZ). **C, D**, Quantification of number of SWDs (**C**) and mean SWD duration (**D**) during an 80 min recording period in uninjected (naive) mice and after injection of vehicle or CBZ (n = 4 per group). **E**, Example EEG traces from WT and TRIP8b KO mice after administration of GBL

(indicated by the black bar under each trace). Asterisks denote seizure onset. **F**, Latency to seizure onset for each genotype (n = 7 WT, 8 KO). **G**, Number of SWDs during a 90-min recording period after GBL administration (n = 5 for each genotype; *p < 0.05, **p < 0.01, ***p < 0.001).

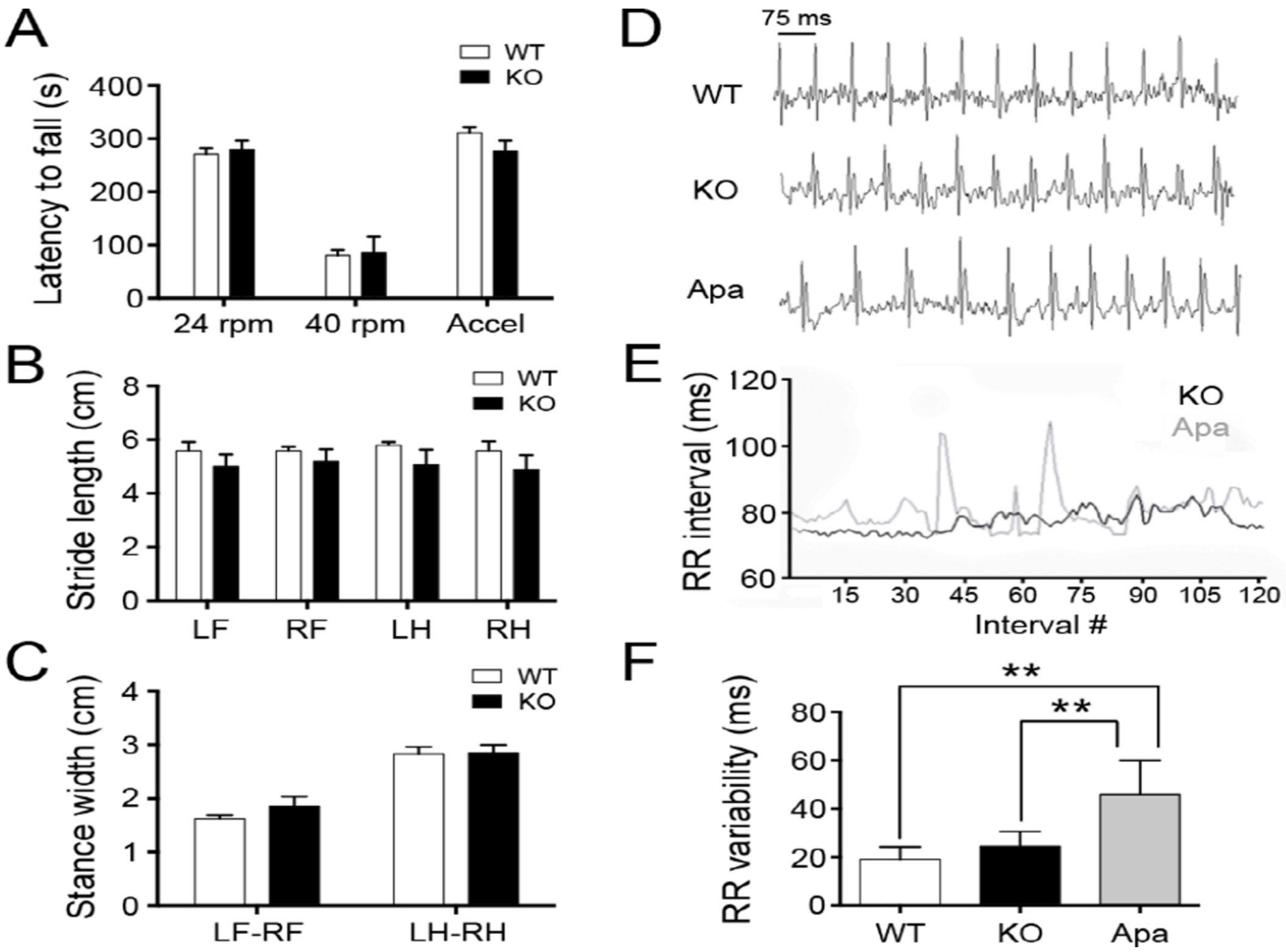

Figure 3.

Motor and cardiac function are unchanged in TRIP8b KO mice. **A**, Latency to fall on 24 rpm, 40 rpm, and accelerating rotarod tests. **B, C**, Measurement of stride length between individual front paws (LF, RF) and hind paws (LH, RH) (**B**) and stance width between front paws (LF-RF) and hind paws (LH-RH) (**C**) as mice walked on a transparent treadmill (n = 7 per genotype). **D**, Representative ECG traces from WT, TRIP8b KO, and *apathetic* mice. **E**, Successive RR intervals of a TRIP8b KO and an *apathetic* mouse, demonstrating high variability in *apathetic* but not TRIP8b KO. **F**, Plot of RR variability for each genotype (n = 4 WT, 3 KO, 3 Apa; **p < 0.01).

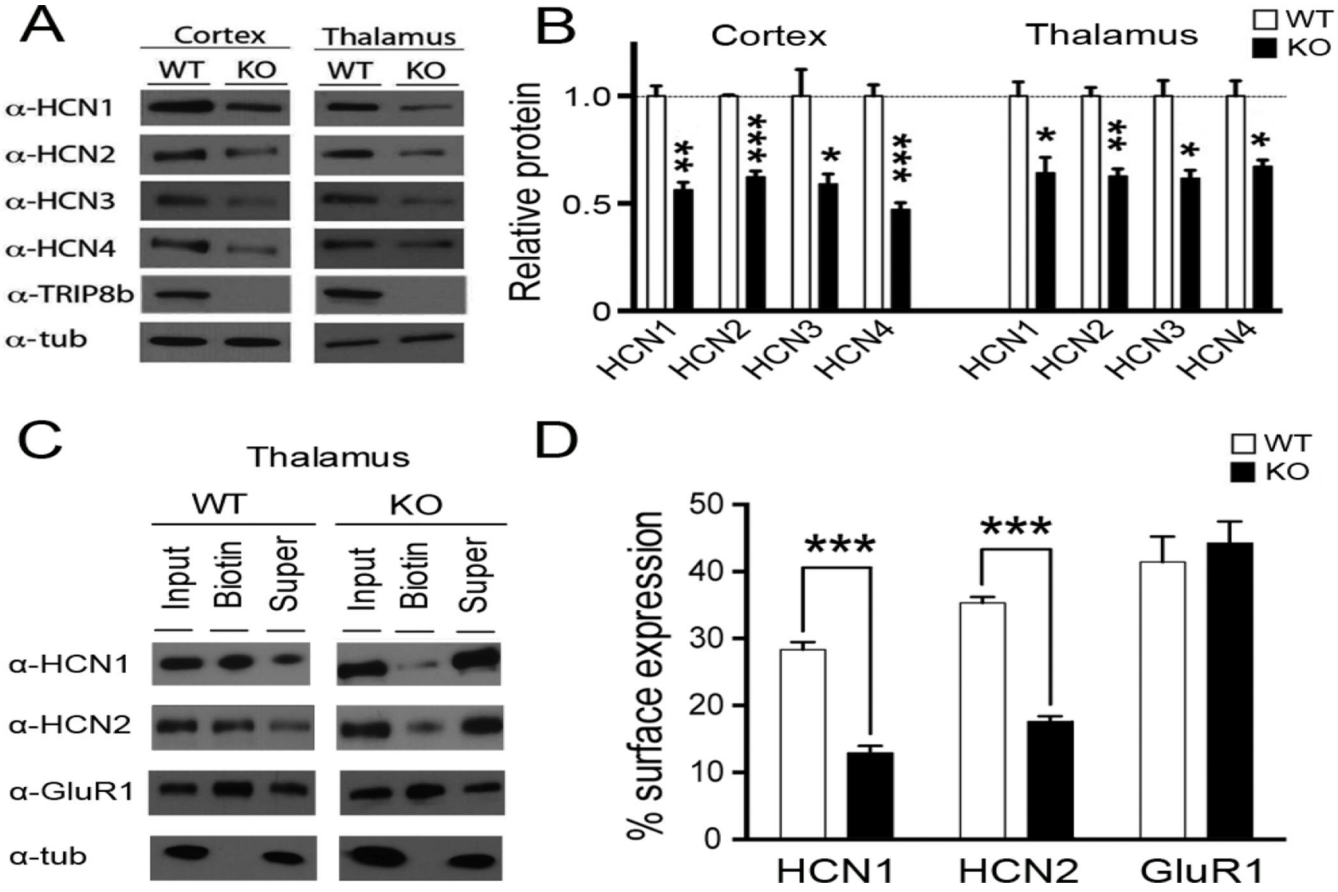

Figure 4.

Reduced overall and surface expression of HCN channel subunits in the cortex and thalamus of TRIP8b KO mice. **A**, Representative western blots from cortical and thalamic lysates prepared from WT and TRIP8b KO mice. **B**, Quantification of protein levels for each subunit in cortex and thalamus (n = 4 per group; *p < 0.05, **p < 0.01, ***p < 0.001; t test with Holm-Bonferroni correction for multiple comparisons). **C**, Representative blots of HCN1, HCN2, GluR1, and β-III-tubulin before (input) and after (biotin) streptavidin precipitation of biotinylated thalamic lysates. Supernatant (super) represents non-surface protein fraction. 30% input was loaded. **D**, Group data of relative surface expression, obtained by normalizing the biotin lane to input lane for each sample (n = 4 for each genotype; ***p < 0.001).

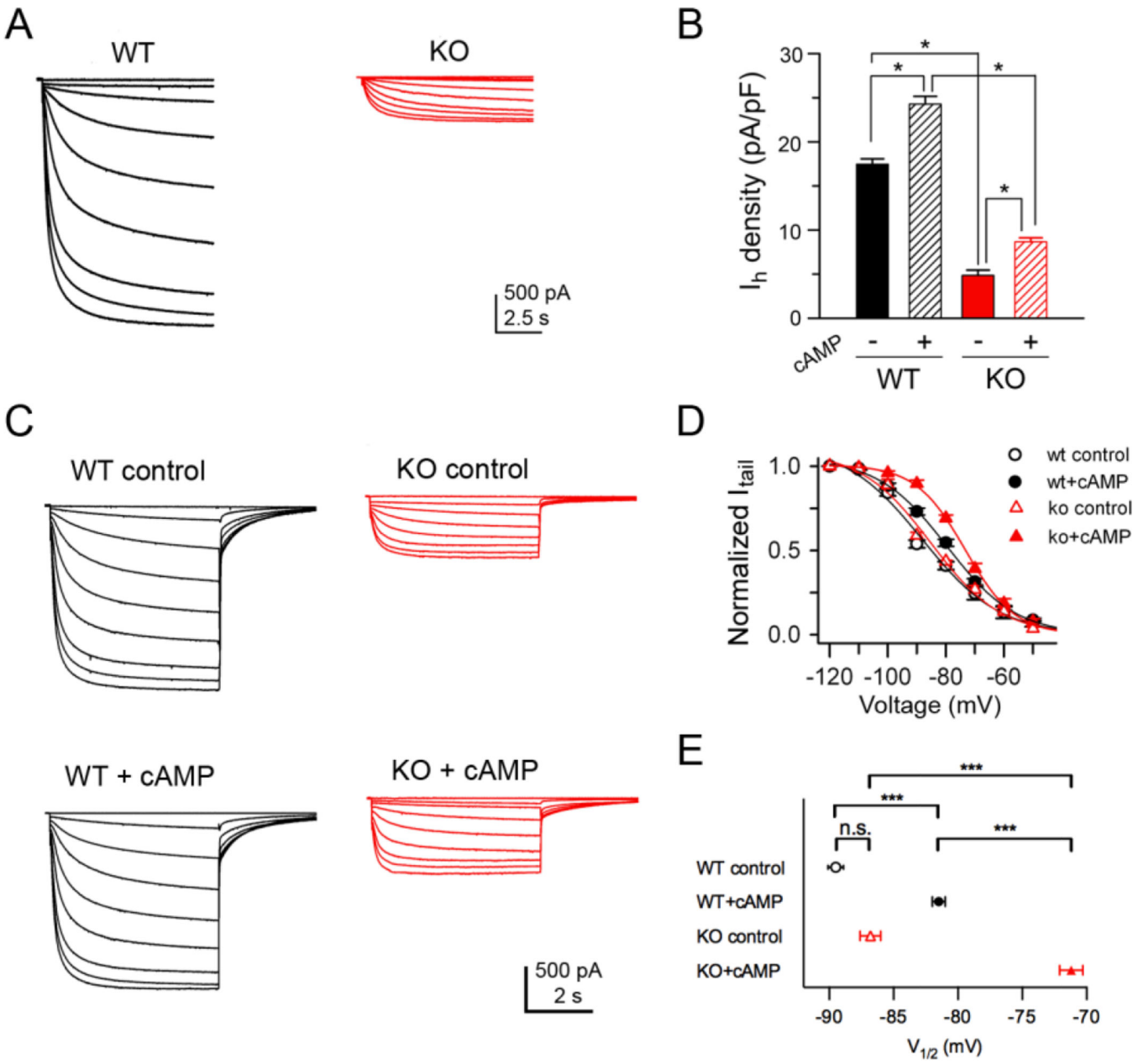

Figure 5.

Deletion of TRIP8b decreases I_h density and enhances cAMP-responsiveness in VB neurons. **A**, Example traces from WT and TRIP8b KO mice recorded in I_h-isolation solution (see Materials and Methods; −50 to −130 mV, 10 s steps). **B**, Comparison of I_h density (at −130 mV) in WT and KO neurons, with and without intracellular 5 μM 8-Br-cAMP (n = 10 per group). **C**, Example traces demonstrating the effect of 5 μM 8-Br-cAMP in each genotype. **D, E**, Comparison of activation curves (**D**) and average $V_{1/2}$ values (**E**) for each condition (WT: n = 20 per group; KO: n = 30 per group; *p < 0.05, ***p < 0.001).

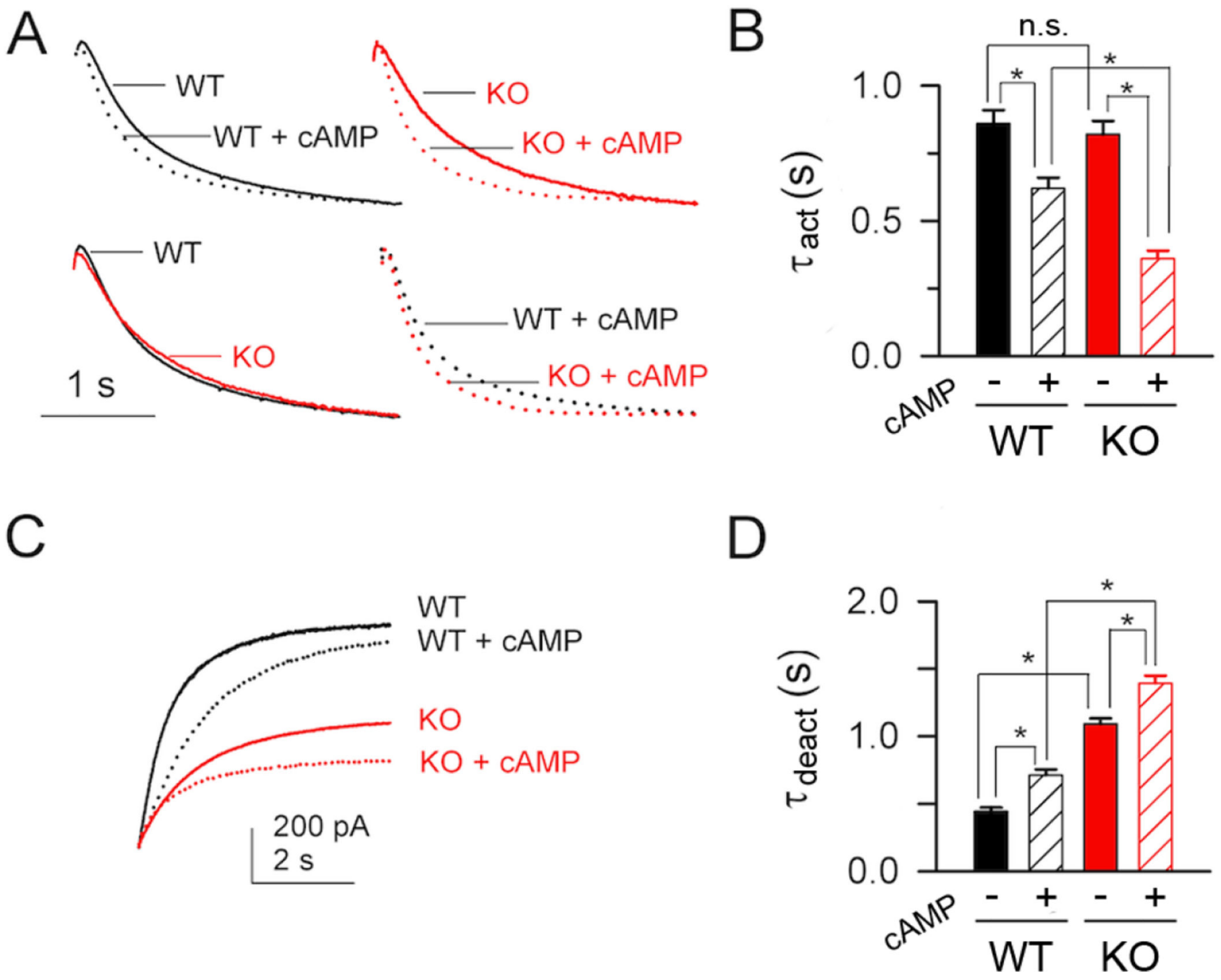

Figure 6.

Effects of TRIP8b deletion on I_h activation and deactivation in VB neurons. **A, B**, Example traces (**A**) and group data (**B**) comparing the effects of genotype and cAMP on I_h activation at −120 mV. Traces are scaled to peak amplitude. **C, D**, Example tail currents (**C**) and time constants of deactivation (**D**) for each condition, recorded at −50 mV after a step to −120 mV (n = 15 per group; *p< 0.05).

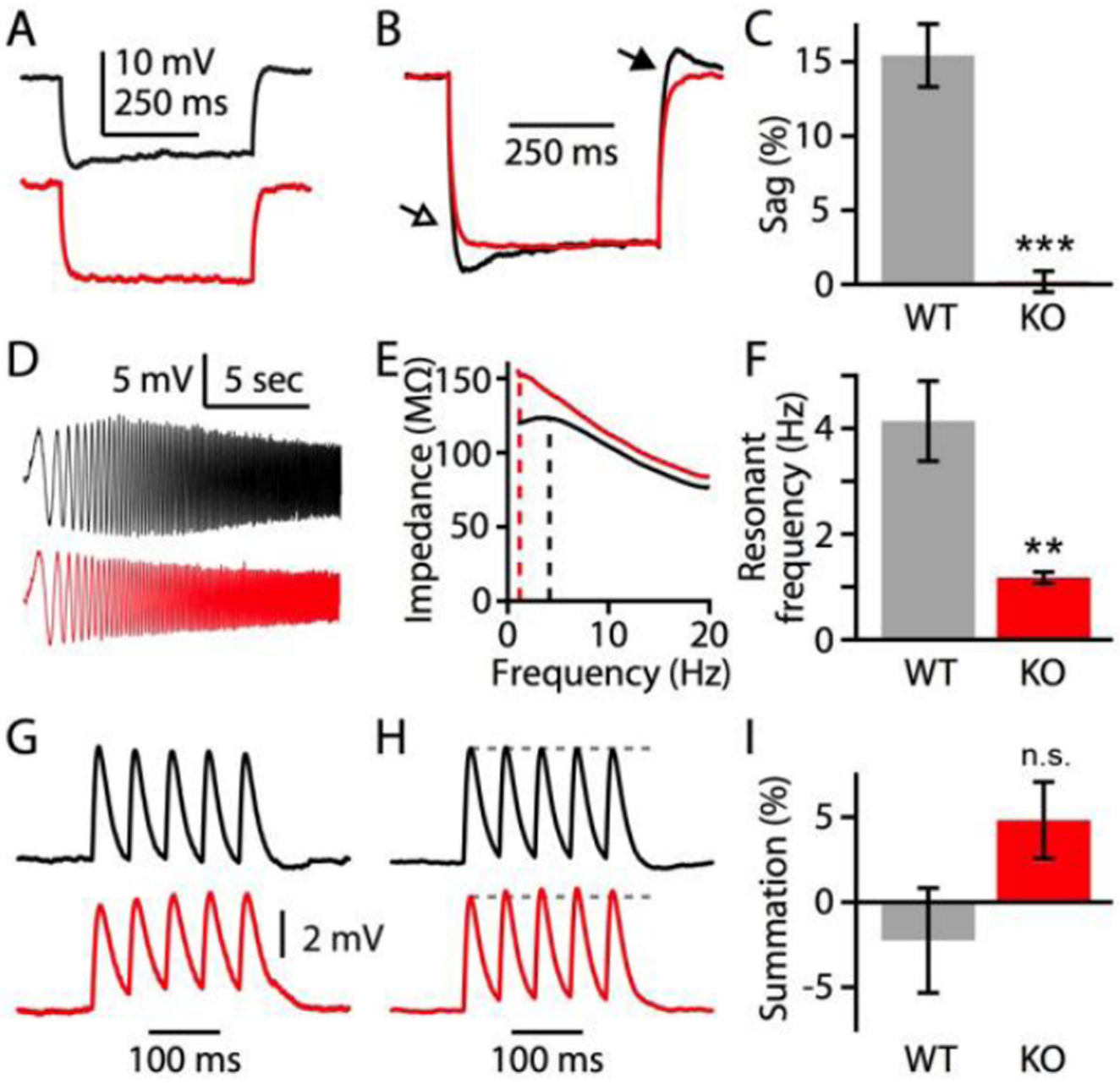

Figure 7.

Deletion of TRIP8b decreases I_h-dependent intrinsic and integrative properties in PT neurons. **A**, Examples of voltage responses to hyperpolarizing current injections (−100 pA, 0.5 sec) recorded in retrogradely labeled PT neurons in neocortical brain slices prepared from WT (black) and KO (red) mice. **B**, Average traces for WT and KO neurons, normalized to the steady-state response, showing lack of membrane potential sag (open arrow) and overshoot (closed arrow) in KO neurons. **C**, Group-averaged sag percentage for WT and KO neurons (n = 11 WT, 9 KO). **D**, Example voltage responses in WT and KO neurons to a chirp stimulus. **E**, Impedance amplitude profiles for WT and KO neurons. Dashed lines indicate resonant frequencies. **F**, Group-averaged resonant frequencies for WT

and KO neurons (n = 8 WT, 7 KO). **G**, Examples of voltage responses in WT and KO neurons to trains of EPSC-like currents injected at the soma. **H**, Average traces for WT and KO neurons, normalized to the amplitude of the first event. **I**, Group-averaged values for summation, calculated as the 5th/1st amplitude ratio (n = 9 WT, 8 KO; **p < 0.01; ***p < .001).

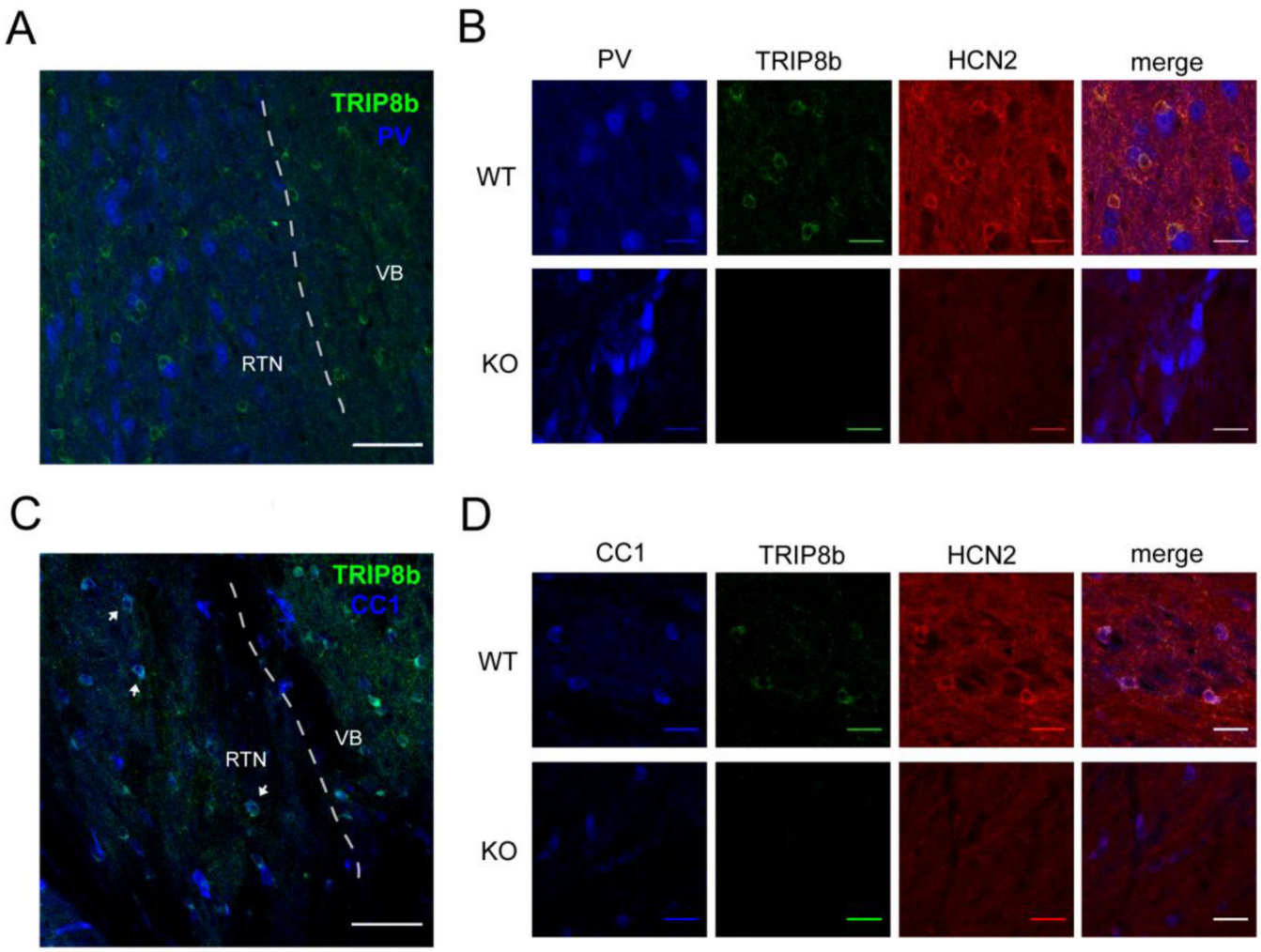

Figure 8.

TRIP8b is coexpressed with CC1 but not parvalbumin (PV) in the RTN. **A, C**, Low-magnification images showing TRIP8b^{+} cells (green) juxtaposed to PV^{+} RTN neurons (blue) in WT mice (**A**). Additional staining identified these cells as CC1^{+} oligodendrocytes (**C**, arrows). Dashed lines indicate the border between RTN and VB thalamus. Scale bars = 50 μm. **B, D**, Higher-magnification images showing co-staining of PV (**B**, blue) or CC1 (**D**, blue) with TRIP8b (green) and HCN2 (red) in the RTN of WT (top) and KO (bottom) mice. Scale bars = 20 μm.

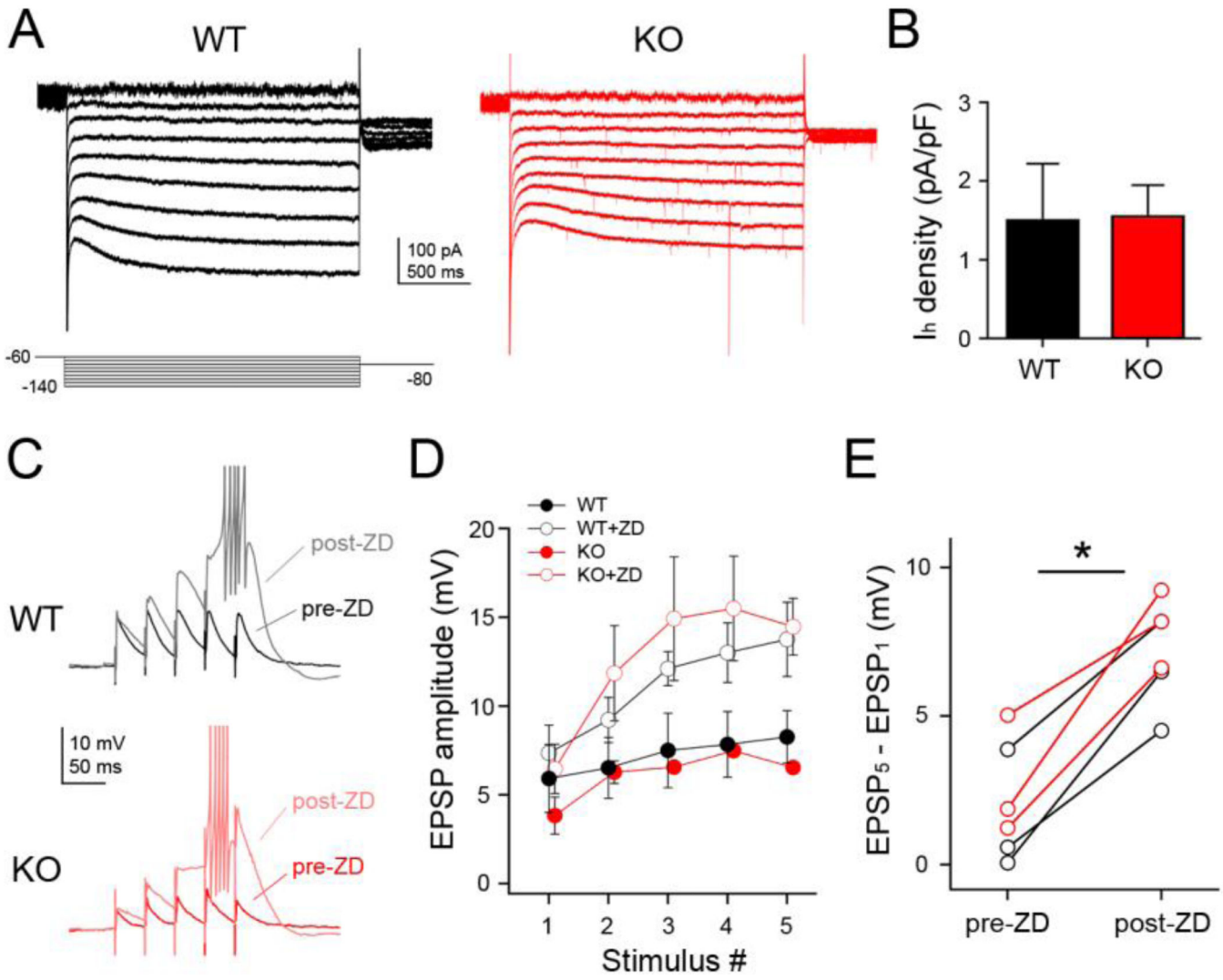

Figure 9.

Deletion of TRIP8b does not affect I_h in RTN neurons. **A**, Example traces from WT and TRIP8b KO RTN neurons during voltage steps from −60 to −140 mV (in the presence of 1 mM Ba^{2+}) **B**, Group-averaged values for I_h density recorded at −130 mV (n = 9 WT, 7 KO). **C**, Example traces from WT and KO RTN neurons during synaptic stimulation (5 stimuli, 30 Hz) before and after application of ZD7288. **D**, Group data of EPSP amplitudes for each condition. **E**, Summation (difference between 5th and 1st EPSPs, see Materials and Methods) before and after ZD7288 (n = 3 for each genotype; *p < 0.05, paired t-test).